Thermal Photons and Lepton Pairs from Quark Gluon Plasma and Hot Hadronic Matter

J. Alam[a,1], S. Sarkar[b], P. Roy[c], T. Hatsuda[a] and B. Sinha[b,c]

a) Physics Department, Kyoto University, Kyoto 606-8502, Japan
b) Variable Energy Cyclotron Centre, 1/AF Bidhan Nagar, Calcutta 700 064 India
c) Saha Institute of Nuclear Physics, 1/AF Bidhan Nagar, Calcutta 700 064 India

Abstract

The formulation of the real and virtual photon production rate from strongly interacting matter is presented in the framework of finite temperature field theory. The changes in the hadronic spectral function induced by temperature are discussed within the ambit of the Walecka type model and QCD sum rule approach. Possibility of observing the direct thermal photon and lepton pair from quark gluon plasma has been contrasted with those from hot hadronic matter without and with medium effects for various mass variation scenarios. We note that the in-medium effects on the low invariant mass distribution of dilepton and transverse momentum spectra of photon are conspicuously visible.

PACS: 25.75.+r;12.40.Yx;21.65.+f;13.85.Qk

1 Introduction

The QCD renormalization group calculation of asymptotic freedom predicts that strongly interacting systems at very high temperature and/or density are composed of weakly interacting quarks and gluons [1, 2, 3]. On the other hand, at low temperature and density the quarks and gluons are confined within the hadrons. Therefore, a phase transition is expected to take place at an intermediate value of temperature and/or density. This transition is actually observed in lattice QCD numerical simulations [4]. A system of thermalized strongly interacting matter where the properties of the system are governed by the quark and gluon degrees of freedom is called Quark Gluon Plasma (QGP). One expects that ultrarelativistic heavy ion collisions (URHIC) might create conditions conducive for the formation and study of QGP [5, 6, 7]. Various model calculations have been performed to look for observable signatures of this state of matter. However, among various signatures of QGP, photons and dileptons are known to be advantageous as these signals probe the entire volume of the plasma, with little interaction and as such are better markers of the space time history of the evolving fireball. This is primarily so because electromagnetic interaction is strong enough to lead to detectable signal, yet it is weak enough to allow the produced particles (real photons and dileptons) to escape the system without further interaction, thus carrying the information

[1] On leave from Variable Energy Cyclotron Centre, 1/AF Bidhan Nagar, Calcutta 700 064, India

of the constituents and their momentum distribution in the thermal bath. The disadvantage with photons is the substantial background from various processes (thermal and non-thermal) [8, 9, 10, 11]. Among these, the contribution from hard QCD processes is well under control in the framework of perturbative QCD and the yield from hadronic decays e. g. $\pi^0/\eta \rightarrow \gamma\,\gamma$ can be estimated by invariant mass analysis. However, photons from the thermalized hadronic gas pose a more difficult task to disentangle. Therefore, it is very important to estimate photons from hot and dense hadronic gas along with the possible modification of the hadronic properties.

In URHIC hadronic matter is formed after a phase transition from QGP. Even if such a phase transition does not occur, realization of hadronic matter at high temperature ($\sim 150 - 200$ MeV) and/or baryon density (a few times normal nuclear matter density) is inevitable. As a result the study of hadronic interactions at high temperature and density assumes great significance. There are several other aspects where medium effects may play an important role. For example spontaneously broken chiral symmetry of the normal hadronic world is expected to be restored at high temperature and density and this will be reflected in the thermal modification of the hadronic spectra [12, 13, 14]. These modifications can be studied by analysing photon, dilepton as well as hadronic spectra.

The real and virtual photon (dilepton) emission rate from QGP is determined by the fundamental theory of strong interaction, QCD. The dominant processes for the photon production from QGP are the annihilation ($q\bar{q} \rightarrow g\gamma$) and Compton processes ($q(\bar{q}) \rightarrow q(\bar{q})\gamma$). The emission rate resulting from these reactions have been evaluated in [15, 16, 17] in the framework of Hard Thermal Loops (HTL) resummation in QCD [18, 19].

However, the progress in our understanding of hot and dense hadronic matter has been retarded since the underlying theory of strong interaction, QCD, is nonperturbative in the low energy regime. Because of this severe constraint considerable amount of work has been done on model building (see e.g. Ref. [20]) in order to study the low energy hadronic states.

Various investigations have addressed the issue of temperature and density dependence of hadronic spectra within different models over the past several years. In particular, in-medium QCD sum rules are useful to make constraints on the hadronic spectral functions at finite temperature and density [21]. Brown and Rho [22] argued that requiring chiral symmetry (in particular the QCD trace anomaly) yields an approximate scaling relation between various effective hadronic masses, $m_N^*/m_N \sim m_\sigma^*/m_\sigma \sim m_{\rho,\omega}^*/m_{\rho,\omega} \sim f_\pi^*/f_\pi$, which implies, that all hadronic masses decrease with temperature. The reduction in ρ meson mass has also been observed in the hidden local symmetry model [23]. The nonlinear sigma model [24, 25], claimed to be the closest low energy description of QCD and the gauged linear sigma model [26] however, shows the opposite trend, *i.e.* m_ρ^* increasing with temperature. The relation between the self energy and the forward scattering amplitude has also been utilized to study the change of hadronic properties in the medium [27, 28].

The change in the masses and decay widths of vector mesons propagating in a medium occurs due to its interaction with the real and virtual excitations in the

medium. In Mean Field Theory (MFT) the condensed scalar field is responsible for the modification of the nucleon mass. In other words, the nucleon mass changes due to the contribution from scalar tadpole diagrams in the nucleon self energy [29, 30]. In the Walecka model approach, the vector meson mass gets shifted due to the decrease of the nucleon mass which appears through thermal loops in the vector meson self energy [31]. The response of the nuclear system to the external probe is characterised by the imaginary part of the vector meson self energy. The interaction of the vector meson with the real particles (on-shell) present in the medium brings in a small change in the mass of the vector meson but the net reduction in the vector meson mass can be attributed to its interaction with the nucleons in the Dirac sea.

Thus, there exists a lot of controversy in the literature about the finite temperature properties of hadrons. In view of this in the present article we consider various scenarios for the shift in the hadronic spectral function at finite temperature and evaluate its effects on the experimentally measurable quantities, the photon and dilepton spectra originating from thermalized system formed after URHIC.

As will be shown in the next section, both the photon and dilepton emission rates are proportional to the retarded electromagnetic current correlation function. These correlators or the spectral functions can be constructed in vacuum from the experimental data obtained in $e^+e^- \rightarrow hadrons$ (or from hadronic decays of τ lepton) for various isovector and isoscalar channels [32, 33]. In-medium spectral function is obtained by modifing the pole and the continuum structure of the vector mesons due its interaction with the constituents of the thermal bath. Due to the lack of understanding of the finite temperature behaviour of scalar and tensor condensates near the critical point, the hadronic properties at non-zero temperature in QCD sum rule approach is not firmly established. In the present article the parameterizations of vector meson masses and the continuum thresholds according to Brown and Rho (BR) and Nambu scaling [34], will be used.

We organize the paper as follows. In section 2 we review the formalism of the emission of real and virtual photons from a thermalized system of strongly interacting particles. In section 3 we introduce the HTL resummation technique and discuss the specific reactions which are used to calculate the photon and dilepton spectra. Section 4 is devoted to discuss the properties of hadrons at finite temperature. The QCD sum rule at finite temperature has been discussed in section 5. We discuss space time evolution dynamics in section 6. In section 7 we present the results of our calculations and finally in section 8, we give a summary and outlook.

2 Electromagnetic Probes - Formulation

The importance of the electromagnetic probes for the thermodynamic state of the evolving matter was first proposed by Feinberg in 1976 [35]. While for most purposes one can calculate the emission rates in a classical framework, Feinberg showed that the emission rates can be related to the electromagnetic current-current correlation function in a thermalized system in a quantum picture and, more importantly, in

a nonperturbative manner. Generally the production of a particle which interacts weakly with the constituents of the thermal bath (the constituents may interact strongly among themselves, the explicit form of their coupling strength is not important) can always be expressed in terms of the discontinuities or imaginary parts of the self energies of that particle [36, 37]. In this section, therefore, we look at the connection between the electromagnetic emission rates (real and virtual photons) and the photon spectral function (which is connected with the discontinuities in self energies) in a thermal system [38], which in turn is connected to the hadronic electromagnetic current-current correlation function [39] through Maxwell equations. It will be shown that the photon emission rate can be obtained from the dilepton emission rate by appropriate modifications.

We begin our discussion with the dilepton production rate. Following Weldon [38] let us define A^μ as the exact Heisenberg photon field which is the source of the leptonic current J^l_μ. To lowest order in the electromagnetic coupling, the S matrix element for the transition $\mid I\rangle \rightarrow \mid H; l^+l^-\rangle$ is given by

$$S_{HI} = e \int \langle H; l^+l^- \mid J^l_\mu(x)\, A^\mu(x) \mid I\rangle \, d^4x \, e^{iq\cdot x}, \tag{2.1}$$

where $\mid I\rangle$ is the initial state corresponding to the two incoming nuclei, $\mid H; l^+l^-\rangle$ is the final state which corresponds to a lepton pair plus anything (hadronic), the parameter e is the renormalized charge and $q = p_1 + p_2$ is the four momentum of the lepton pair. Since we assume that the lepton pair does not interact with the emitting system, the matrix element can be factorized in the following way

$$\langle H; l^+l^- \mid J^l_\mu(x)\, A^\mu(x) \mid I\rangle = \langle H \mid A^\mu(x) \mid I\rangle \langle\, l^+l^- \mid J^l_\mu(x) \mid 0\rangle. \tag{2.2}$$

Putting the explicit form of the current J^l_μ in terms of the Dirac spinors we obtain

$$S_{HI} = e\, \frac{\bar{u}(p_1)\gamma_\mu\, v(p_2)}{V\sqrt{2E_1 2E_2}} \int d^4x\, e^{iq\cdot x} \langle H \mid \; A^\mu(x) \mid I\rangle. \tag{2.3}$$

The dilepton multiplicity from a thermal system is obtained by summing over the final states and averaging over the initial states with a weight factor $Z(\beta)^{-1}\, e^{-\beta\, E_I}$ to get

$$N = \frac{1}{Z(\beta)} \sum_I \sum_H \mid S_{HI} \mid^2 \; e^{-\beta\, E_I} \frac{V\, d^3p_1}{(2\pi)^3} \, \frac{V\, d^3p_2}{(2\pi)^3}, \tag{2.4}$$

where E_I is the total energy in the initial state. After some algebra N can be written in a compact form as follows

$$N = e^2\, L^{\mu\nu}\, H_{\mu\nu} \frac{d^3p_1}{(2\pi)^3 E_1} \, \frac{d^3p_2}{(2\pi)^3 E_2}, \tag{2.5}$$

where $L_{\mu\nu}$ is the leptonic tensor given by

$$\begin{aligned} L^{\mu\nu} &= \frac{1}{4} \sum_{spins} \bar{u}(p_1)\gamma^\mu\, v(p_2)\bar{v}(p_2)\gamma^\nu\, u(p_1) \\ &= p_1^\mu\, p_2^\nu + p_2^\mu\, p_2^\nu - \frac{q^2}{2}\, g^{\mu\nu}, \end{aligned} \tag{2.6}$$

and $H_{\mu\nu}$ is the photon tensor

$$H_{\mu\nu} = \frac{1}{Z(\beta)}\, e^{-\beta\, q_0} \int d^4x\, d^4y\, e^{iq\cdot(x-y)} \sum_H \langle H \mid A_\mu(x)\, A_\nu(y) \mid H\rangle\, e^{-\beta\, E_H}. \tag{2.7}$$

To obtain the above equation we have used the resolution of identity $1 = \sum_I \mid I\rangle\langle I \mid$ and the energy conservation equation $E_I = E_H + q_0$, where q_0 is the energy of the lepton pair and E_H is the energy of the rest of the system. Using translational invariance of the matrix element we can write

$$H_{\mu\nu} = \Omega\, e^{-\beta\, q_0} D^{>}_{\mu\nu}, \tag{2.8}$$

where Ω is the four volume of the system and $D^{>}_{\mu\nu}$ is defined through the following relations. The photon propagator $\mathbf{D}_{\mu\nu}$ in the real time formalism has a (2×2) matrix structure [40, 41]. The time ordered propagator is the $(1,1)$ component of $\mathbf{D}_{\mu\nu}$ (see later). In coordinate space it is defined as

$$\begin{aligned} iD^{11}_{\mu\nu}(x) &= \frac{1}{Z(\beta)} \sum_H \langle H \mid T\{A_\mu(x)\, A_\nu(0)\} \mid H\rangle\, e^{-\beta\, E_H} \\ &= \theta(x_0) D^{>}_{\mu\nu}(x) + \theta(-x_0) D^{<}_{\nu\mu}(x). \end{aligned} \tag{2.9}$$

In momentum space it takes the form [42]

$$D^{11}_{\mu\nu}(q_0,\vec{q}) = \int_{-\infty}^{\infty} \frac{d\omega}{2\pi} \left[\frac{D^{>}_{\mu\nu}(\omega,\vec{q})}{q^0-\omega+i\epsilon} - \frac{D^{<}_{\nu\mu}(\omega,\vec{q})}{q^0-\omega-i\epsilon}\right]. \tag{2.10}$$

Using the Kubo Martin Schwinger (KMS) relation in momentum space,

$$D^{>}_{\mu\nu}(\omega,\vec{q}) = e^{\beta q_0} D^{<}_{\nu\mu}(\omega,\vec{q}), \tag{2.11}$$

we have

$$D^{>}_{\mu\nu}(q_0,\vec{q}) = \frac{2}{1+e^{-\beta q_0}} \mathrm{Im} D^{11}_{\mu\nu}(q_0,\vec{q}). \tag{2.12}$$

The rate of dilepton production per unit volume (N/Ω) is then given by

$$\frac{dN}{d^4x} = \frac{2e^2}{e^{\beta q_0}+1}\, L^{\mu\nu} \mathrm{Im} D^{11}_{\mu\nu}(q_0,\vec{q}) \frac{d^3p_1}{(2\pi)^3 E_1} \frac{d^3p_2}{(2\pi)^3 E_2}. \tag{2.13}$$

Now the spectral function of the (virtual) photon in the thermal bath is conventionally defined as

$$\rho_{\mu\nu}(q_0,\vec{q}) = \frac{1}{2\pi Z(\beta)} \int d^4x\, e^{iq\cdot x} \sum_H \langle H \mid [A_\mu(x), A_\nu(0)] \mid H\rangle e^{-\beta\, E_H}, \tag{2.14}$$

so that, we have [37, 42]

$$D^{11}_{\mu\nu}(q_0,\vec{q}) = \int_{-\infty}^{\infty} d\omega \frac{\rho_{\mu\nu}(\omega,\vec{q})}{q_0-\omega+i\epsilon} - 2i\pi f_{BE}(q_0)\rho_{\mu\nu}(q_0,q), \tag{2.15}$$

where $f_{BE}(q_0) = [e^{\beta q_0} - 1]^{-1}$. This leads to

$$\mathrm{Im}D^{11}_{\mu\nu}(q_0, \vec{q}) = \pi[1 + 2f_{BE}(q_0)]\rho_{\mu\nu}(q_0, \vec{q}). \tag{2.16}$$

In terms of the photon spectral function the dilepton emission rate is obtained as

$$\frac{dN}{d^4x} = 2\pi e^2 L^{\mu\nu}\rho_{\mu\nu}(q_0, \vec{q})\frac{d^3p_1}{(2\pi)^3 E_1}\frac{d^3p_2}{(2\pi)^3 E_2} f_{BE}(q_0). \tag{2.17}$$

This relation which expresses the dilepton emission rate in terms of the spectral function of the photon in the medium is an important result.

As is well known, it is not the time-ordered propagator that has the required analytic properties in a heat bath, but rather the retarded one. We thus introduce the retarded propagator which will enable us to express the dilepton rate in terms of the retarded photon self energy. The retarded photon propagator is defined as

$$iD^R_{\mu\nu}(q_0, \vec{q}) = \frac{1}{Z(\beta)}\int d^4x\, e^{iq\cdot x}\theta(x_0)\sum_H \langle H \mid [A_\mu(x), A_\nu(0)] \mid H\rangle e^{-\beta E_H}, \tag{2.18}$$

which leads to the relation

$$\rho_{\mu\nu} = -\frac{1}{\pi}\mathrm{Im}D^R_{\mu\nu}. \tag{2.19}$$

The above equation implies that to evaluate the spectral function at $T \neq 0$ we need to know the imaginary part of the retarded propagator. It is interesting to note that the above expression for spectral function reduces to its vacuum value as $\beta \to \infty$ since the only state which enters in the spectral function is the vacuum [43].

Consequently we have

$$\frac{dN}{d^4x} = -2e^2 L^{\mu\nu}\mathrm{Im}D^R_{\mu\nu}(q_0, \vec{q})\frac{d^3p_1}{(2\pi)^3 E_1}\frac{d^3p_2}{(2\pi)^3 E_2} f_{BE}(q_0). \tag{2.20}$$

This result can also be derived directly from Eq. 2.13 using the relation [40],

$$\mathrm{Im}\, D^{11}_{\mu\nu} = (1 + 2f_{BE})\mathrm{Im}\, D^R_{\mu\nu}. \tag{2.21}$$

Now the exact retarded propagator can be expressed in terms of the proper self energy through the Dyson-Schwinger equation:

$$D^R_{\mu\nu} = -\frac{A_{\mu\nu}}{q^2 + \Pi^R_T} - \frac{B_{\mu\nu}}{q^2 + \Pi^R_L} + (\zeta - 1)\frac{q_\mu\, q_\nu}{q^4}, \tag{2.22}$$

where $A^{\mu\nu}$ and $B^{\mu\nu}$ are transverse and longitudinal projection tensors respectively(to be defined later) and Π^R_T and Π^R_L are the transverse and longitudinal components of the retarded proper photon self energy. The presence of the parameter ζ indicates the gauge dependence of the propagator. Although the gauge dependence cancels out in the calculation of physical quantities, one should, however, be careful when extracting physical quantities from the propagator directly, especially in the non-abelian gauge theory.

Inserting the imaginary part of the retarded photon propagator from Eq. 2.22 in Eq. 2.20 we get

$$\frac{dN}{d^4x} = 2\pi\, e^2\, L_{\mu\nu}(A^{\mu\nu}\rho_T \,+\, B^{\mu\nu}\,\rho_L)\frac{d^3p_1}{(2\pi)^3E_1}\,\frac{d^3p_2}{(2\pi)^3E_2}\,f_{BE}(q_0), \tag{2.23}$$

with

$$\rho_{T,L} = -\frac{1}{\pi}\frac{\mathrm{Im}\,\Pi^R_{T,L}}{(q^2+\mathrm{Re}\,\Pi^R_{T,L})^2+(\mathrm{Im}\,\Pi^R_{T,L})^2}. \tag{2.24}$$

Comparing with Eq. 2.17 we have

$$\rho^{\mu\nu} = A^{\mu\nu}\rho_T + B^{\mu\nu}\rho_L. \tag{2.25}$$

It has been argued by Weldon [44] that the electromagnetic plasma resonance occurring through the spectral function derived above could be a signal of the deconfinement phase transition provided the plasma life time is long enough for the establishment of the resonance. Using the relation

$$\begin{aligned}\int \prod_{i=1,2}\frac{d^3p_i}{(2\pi)^3E_i}\delta^4(p_1+p_2-q)\,L^{\mu\nu}(p_1,p_2) &= \frac{1}{(2\pi)^6}\frac{2\pi}{3}(q^\mu\,q^\nu - q^2\,g^{\mu\nu}) \\ &\times \;(1+\frac{2m^2}{q^2})\sqrt{1-\frac{4m^2}{q^2}},\end{aligned} \tag{2.26}$$

and

$$\begin{aligned} q^\mu A_{\mu\nu} &= 0 \\ q^\mu B_{\mu\nu} &= 0 \\ g^{\mu\nu}A_{\mu\nu} &= 2 \\ g^{\mu\nu}B_{\mu\nu} &= 1, \end{aligned} \tag{2.27}$$

the dilepton rate is finally obtained as

$$\frac{dR}{d^4q} = -\frac{\alpha}{12\pi^3}q^2(1+\frac{2m^2}{q^2})\sqrt{1-\frac{4m^2}{q^2}}(2\rho_T+\rho_L)f_{BE}(q_0), \tag{2.28}$$

where m is the lepton mass. This is the *exact* expression for the dilepton emission rate from a thermal medium of interacting particles.

The emission rate of dilepton can also be obtained in terms of the electromagnetic current-current correlation function [39]. Denoting the hadronic part of the electromagnetic current operator by J^h_μ, the leptonic part by J^l_ν and the free photon propagator by $D^{\mu\nu}$, we have the matrix element for this transition :

$$S_{HI} = e\langle\, H; l^+\, l^-\, \mid \int d^4x d^4y J^l_\mu(x) D^{\mu\nu}(x-y)\, J^h_\nu(y) \mid I\rangle. \tag{2.29}$$

This obviously follows from Eq. 2.1 by realising that the solution of the equation of motion of the interacting photon field is

$$A^\mu(x) = \int d^4y D^{\mu\nu}(x-y)J^h_\nu(y). \tag{2.30}$$

As in the earlier case the leptonic part of the current can be easily factored out. Writing the Fourier transform of photon propagator and squaring the matrix elements, one obtains the rate of dilepton production

$$dR = e^2\, L^{\mu\nu}\, W^{>}_{\mu\nu}\, \frac{e^{-\beta q_0}}{q^4}\, \frac{d^3\, p_1}{(2\pi)^3\, E_1}\, \frac{d^3\, p_2}{(2\pi)^3\, E_2}, \tag{2.31}$$

where $W^{>}_{\mu\nu}(q)$ is the Fourier transform of the thermal expectation value of the electromagnetic current-current correlation function:

$$W^{>}_{\mu\nu} = \int d^4x e^{iqx} \sum_H \langle H \mid J^h_\mu(x) J^h_\nu(0) \mid H \rangle\, \frac{e^{-\beta\, E_H}}{Z}. \tag{2.32}$$

The subtleties of the thermal averaging have been elucidated earlier. It is thus readily seen (Eq. 2.31) that the dilepton and photon data yields considerable information about the thermal state of the hadronic system; at least the full tensor structure of $W^{\mu\nu}$ can in principle be determined. The most important point to realize here is that the analysis is essentially nonperturbative up to this point.

The connection between the electromagnetic current-current correlation and the spectral function can be expressed in a straight forward way by substituting J^h_μ and J^h_ν using Maxwell equation $(\partial_\alpha \partial^\alpha\, A_\mu - \zeta^{-1}(\zeta - 1)\partial_\mu\, (\partial_\alpha\, A^\alpha) = J^h_\mu)$ in Eq. 2.32 to obtain

$$\begin{aligned} W^{>}_{\mu\nu} &= \left(q^2 g_{\mu\alpha} - \frac{\zeta - 1}{\zeta} q_\mu q_\alpha\right) D^{\alpha\beta}_{>} \left(q^2 g_{\beta\nu} - \frac{\zeta - 1}{\zeta} q_\beta q_\nu\right) \\ &= 2\pi \left(q^2 g_{\mu\alpha} - \frac{\zeta - 1}{\zeta} q_\mu q_\alpha\right) \rho^{\alpha\beta} \left(q^2 g_{\beta\nu} - \frac{\zeta - 1}{\zeta} q_\beta q_\nu\right) (1 + f_{BE}). \end{aligned} \tag{2.33}$$

Using the last equation in Eq. 2.31 we can recover Eq. 2.17. This establishes the connection between the two approaches of Refs.[38, 39].

In most of the cases the dilepton production rate from a thermal system is calculated with the approximation $\Pi^R_T = \Pi^R_L \equiv \Pi^R$. Since $\Pi^R_{L,T}$ and $\Pi^R_{L,T}$ are both proportional to α (the fine structure constant) they are small for all practical purposes (this corresponds to the free propagation of the virtual photon in the thermal bath). Therefore $\rho_{L,T}(\equiv \rho)$ is given by

$$\rho = -\frac{1}{\pi} \frac{\mathrm{Im}\, \Pi^R}{q^4} = -\frac{1}{\pi} \frac{\mathrm{Im}\Pi^{R\mu}_\mu}{3q^4}. \tag{2.34}$$

Using this in Eq. 2.28 we get

$$\frac{dR}{d^4q} = \frac{\alpha}{12\pi^4\, q^2} (1 + \frac{2m^2}{q^2}) \sqrt{1 - \frac{4m^2}{q^2}}\, \mathrm{Im}\Pi^{R\mu}_\mu\, f_{BE}(q_0). \tag{2.35}$$

This is the familiar result most widely used for the dilepton emission rate [37]. It must be emphasized that this relation is valid only to $O(e^2)$ since it does not

account for the possible reinteractions of the virtual photon on its way out of the bath. The possibility of emission of more than one photon has also been neglected here. However, the expression is true to all orders in strong interaction.

The electromagnetic decay of unstable particles (*e.g.* ρ, ω and ϕ) within a thermal system could provide valuable information about the nature of the system. In a thermal medium the production of an off-shell vector meson (V) of four momentum q (where $q^2 = M^2$) and its subsequent decay into a lepton pair leads to the dilepton emission rate as [45]

$$dR = \frac{2M}{(2\pi)^3}\rho^V_{\mu\nu}\, P^{\mu\nu}\, f_{BE}(q_0)\Gamma_{V\to l^+l^-}\, d^4q, \tag{2.36}$$

where $\rho^V_{\mu\nu}$ is the spectral function of the off-shell vector meson given by Eq. 2.14 with the photon field replaced by the interpolating fields for vector mesons, the exact form of which is not important in the present case, $P_{\mu\nu}(=\sum \epsilon_\mu\, \epsilon^*_\nu) = -g_{\mu\nu} + q_\mu q_\nu/q^2$ is the projection operator for the vector meson V and $\Gamma_{V\to l^+l^-}$ is the partial decay width for the process $V \to l^+l^-$ in vacuum. The spectral function is expressed in terms of the retarded vector meson propagator (as has been done before in Eq. 2.19 in case of photon). In the limit $\Pi^R_T = \Pi^R_L = \Pi^R$, the spectral function is given by

$$\rho^V_{\mu\nu} = \frac{1}{\pi}\frac{\mathrm{Im}\Pi^R}{(q^2 - m_V^2 + \mathrm{Re}\Pi^R)^2 + (\mathrm{Im}\Pi^R)^2}\, P_{\mu\nu}. \tag{2.37}$$

Using the relation $P^{\mu\nu}\, P_{\mu\nu} = (2J+1)$, we get the dilepton emission rate due to the decay of an unstable vector meson of spin J as

$$\frac{dR}{d^4q} = 2\frac{(2J+1)}{(2\pi)^3}\, f_{BE}\, M\Gamma_{V\to l^+l^-}\, \left[\frac{1}{\pi}\frac{\mathrm{Im}\Pi^R}{(q^2 - m_V^2 + \mathrm{Re}\Pi^R)^2 + (\mathrm{Im}\Pi^R)^2}\right], \tag{2.38}$$

where $\mathrm{Im}\,\Pi^R$ is the imaginary part of the self energy of particle V which should be calculated within the framework of thermal field theory [46]. For a particle which does not decay in the collision volume (the total width $\Gamma_{\rm tot} = \mathrm{Im}\Pi^R/M$ is small) the spectral function in the above equation (term within the square bracket) becomes $\delta(q^2 - m_V^2)$, as it should be for a stable particle. In a medium the width $\Gamma_{\rm tot}$ for V should be calculated with all the processes involving the creation and annihilation of V, *i.e.* $\Gamma_{\rm tot} = \Gamma_{V\to \rm all} - \Gamma_{\rm all\to V}$ [45].

To obtain the real photon emission rate per unit volume (dR) from a system in thermal equilibrium we note that the dilepton emission rate differs from the photon emission rate in the following way. The factor $e^2\, L_{\mu\nu}/q^4$ which is the product of the electromagnetic vertex $\gamma^* \to l^+\, l^-$, the leptonic current involving Dirac spinors and the square of the photon propagator should be replaced by the factor $\sum \epsilon_\mu\, \epsilon_\nu (= -g_{\mu\nu})$ for the real (on-shell) photon. Finally the phase space factor $d^3p_1/[(2\pi)^3\, E_1]\, d^3p_2/[(2\pi)^3 E_2]$ should be replaced by $d^3q/[(2\pi)^3 q_0]$ to obtain

$$dR = -\frac{e^{-\beta q_0}}{2(2\pi)^3}\, g^{\mu\nu}\, W^>_{\mu\nu}\, \frac{d^3q}{q_0}. \tag{2.39}$$

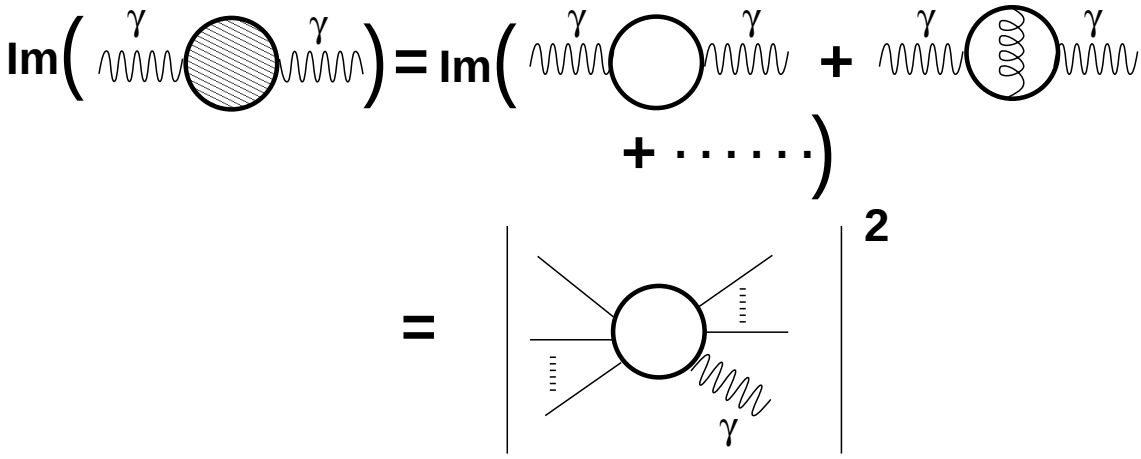

Figure 1: Optical Theorem in Quantum Field Theory

The current-current correlation function $W^{>}_{\mu\nu}$ is related to the retarded correlator by [47]

$$W^{>}_{\mu\nu} = 2e^{\beta q_0} f_{BE}(q_0) \mathrm{Im} W^{R}_{\mu\nu} \tag{2.40}$$

where

$$\begin{aligned} W^{R}_{\mu\nu} &= i \int d^4x e^{iqx} \theta(x_0) \sum_H \langle H \mid J^h_\mu(x) J^h_\nu(0) \mid H \rangle \frac{e^{-\beta E_H}}{Z}, \\ &= -\Pi^{R}_{\mu\nu}. \end{aligned} \tag{2.41}$$

$\Pi^{R}_{\mu\nu}$ in the above is the retarded improper self energy of the photon. However, to $O(e^2)$, the improper and proper self energies are equal [47, 48], so that

$$q_0 \frac{dR}{d^3q} = \frac{g^{\mu\nu}}{(2\pi)^3} \mathrm{Im}\Pi^{R}_{\mu\nu} f_{BE}(q_0). \tag{2.42}$$

This result can also be obtained directly from Eq. 2.35. The emission rate given above is correct up to order e^2 in electromagnetic interaction but exact, in principle, to all order in strong interaction. However, for all practical purposes one is able to evaluate up to a finite order of loop expansion. Now it is clear from the above results that to evaluate photon and dilepton emission rate from a thermal system we need to evaluate the imaginary part of the photon self energy. The Cutkosky rules at finite temperature or the thermal cutting rules [40, 49, 50] give a systematic procedure to calculate the imaginary part of a Feynman diagram. The Cutkosky rule expresses the imaginary part of the n-loop amplitude in terms of physical amplitude of lower order ($n-1$ loop or lower). This is shown schematically in Fig. (1). When the imaginary part of the self energy is calculated up to and including L order loops where L satisfies $x + y < L + 1$, then one obtains the photon emission rate for the reaction x particles $\rightarrow y$ particles $+ \gamma$ and the above formalism becomes equivalent to the relativistic kinetic theory formalism [51].

For a reaction $1 + 2 \rightarrow 3 + \gamma$ the photon (of energy E) emission rate is given by [52]

$$E\frac{dR}{d^3p} = \frac{\mathcal{N}}{16(2\pi)^7 E}\int_{(m_1+m_2)^2}^{\infty} ds \int_{t_{\min}}^{t_{\max}} dt\,|\mathcal{M}|^2 \int dE_1 \times \int dE_2 \frac{f(E_1)\,f(E_2)\,[1+f(E_3)]}{\sqrt{aE_2^2+2bE_2+c}}, \tag{2.43}$$

where

$$\begin{aligned}
a &= -(s+t-m_2^2-m_3^2)^2 \\
b &= E_1(s+t-m_2^2-m_3^2)(m_2^2-t)+E[(s+t-m_2^2-m_3^2)(s-m_1^2-m_2^2) \\
&\quad -2m_1^2(m_2^2-t)] \\
c &= -E_1^2(m_2^2-t)^2-2E_1E[2m_2^2(s+t-m_2^2-m_3^2)-(m_2^2-t)(s-m_1^2-m_2^2)] \\
&\quad -E^2[(s-m_1^2-m_2^2)^2-4m_1^2m_2^2]-(s+t-m_2^2-m_3^2)(m_2^2-t) \\
&\quad \times(s-m_1^2-m_2^2)+m_2^2(s+t-m_2^2-m_3^2)^2+m_1^2(m_2^2-t)^2 \\
E_{1\min} &= \frac{(s+t-m_2^2-m_3^2)}{4E}+\frac{Em_1^2}{s+t-m_2^2-m_3^2} \\
E_{2\min} &= \frac{Em_2^2}{m_2^2-t}+\frac{m_2^2-t}{4E} \\
E_{2\max} &= -\frac{b}{a}+\frac{\sqrt{b^2-ac}}{a}.
\end{aligned}$$

In a similar way the dilepton emission rate for a reaction $a\,\bar{a} \rightarrow l^+\,l^-$ can be obtained as

$$\frac{dR}{d^4q} = \int \frac{d^3p_a}{2E_a(2\pi)^3}f(p_a)\int \frac{d^3p_{\bar{a}}}{2E_{\bar{a}}(2\pi)^3}f(p_{\bar{a}})\int \frac{d^3p_1}{2E_1(2\pi)^3}\int \frac{d^3p_2}{2E_2(2\pi)^3} \mid \mathcal{M} \mid^2_{a\bar{a}\rightarrow l^+l^-} (2\pi)^4\delta^{(4)}(p_a+p_{\bar{a}}-p_1-p_2)\delta^{(4)}(q-p_a-p_{\bar{a}}). \tag{2.44}$$

where $f(p_a)$ is the appropriate occupation probability for bosons or fermions. The Pauli blocking of the lepton pair in the final state has been neglected in the above equation.

3 Photon and Dilepton Emission Rate

In this section we briefly discuss the HTL resummation technique and the specific reactions considered in the present work to evaluate the electromagnetic probes from QGP as well as hadronic matter.

3.1 Photon emission from QGP in the HTL approximation

The thermal photon emission rate from QGP is governed by the following Lagrangian density

$$\mathcal{L}_{QGP} = \mathcal{L}_{QCD} + \mathcal{L}_{\gamma q}, \tag{3.1}$$

where

$$\begin{aligned}\mathcal{L}_{QCD} &= -\frac{1}{4}\sum_{a=1}^{8} G^a_{\mu\nu}G^{a\mu\nu} + \sum_{f=1}^{N_f}\bar{\psi}_f(i\partial\!\!\!/ - g_s\gamma^\mu G^a_\mu\frac{\lambda^a}{2})\psi_f,\\ \mathcal{L}_{\gamma q} &= -\frac{1}{4}F_{\mu\nu}F^{\mu\nu} - \sum_{f=1}^{N_f} e_f\bar{\psi}_f\gamma^\mu A_\mu\psi_f. \end{aligned} \tag{3.2}$$

In the above, G^a_μ, A_μ and ψ_f are the gluon, photon and quark fields respectively. As mentioned in the introduction the dominant processes for the photon production from QGP are the annihilation ($q\bar{q} \to g\gamma$) and Compton processes ($q(\bar{q}) \to q(\bar{q})\gamma$). However, the production rate from these processes diverge due to the exchange of massless particles. This is a well-known problem in thermal perturbative expansion of non-abelian gauge theory which suffers from infra-red divergences. One type of the divergences could be cured by taking into account the 'electric type' screening through the Hard Thermal Loops (HTL) approximation [18]. The perturbation theory also contains 'magnetic type' divergences, which can be eliminated if there is a screening of the magnetic field [53, 54, 55]. Magnetic screening is relevant if any physical quantity is sensitive to the scale g_s^2T. In the present work we consider the production of hard photons ($E \geq T$). For such cases the infra-red divergences could be eliminated within the framework of HTL.

The theory of HTL begins with the observation that at non-zero temperature there are two energy scales - one associated with the temperature T, called the hard scale and the other connected with the fermionic mass $\sim g_sT$ ($g_s << 1$), induced by the temperature, known as the soft scale. A momentum p^μ appearing in the self energy diagram of photon would be called soft (hard) if both the temporal and the spatial components are $\sim g_sT$ (any component is $\sim T$). If any physical quantity is sensitive to the soft scale then HTL resummation becomes essential, *i.e.* in such cases the correlation functions has to be expanded in terms of the effective vertices and propagators, where the effective quantities are the corresponding bare quantities plus the high temperature limit of one loop corrections.

The notion of HTL can be clearly demonstrated in massless ϕ^4 theory in the following way. Consider the Lagrangian density

$$\mathcal{L} = \frac{1}{2}(\partial\phi)^2 - g^2\phi^4. \tag{3.3}$$

The thermal mass resulting from the one loop tadpole diagram in this model is $m_{\rm th} \sim g^2T^2$. At soft momentum scale ($p^\mu \sim gT$) the inverse of the bare propagator goes as $\sim g^2T^2$. Thus, the one loop (tadpole) correction is as large as the tree amplitude. Therefore, this tadpole is a HTL by definition. Braaten and Pisarski [18] have argued that these HTL contributions should be taken into account consistently by re-ordering the perturbation series in terms of effective vertices and propagators. Therefore, according to their prescription we have

$$\mathcal{L} = \frac{1}{2}(\partial\phi)^2 - g^2\phi^4 - m^2_{\rm th}\phi^2 + m^2_{\rm th}\phi^2 = \mathcal{L}_{\rm eff} + \mathcal{L}_{\rm ct}, \tag{3.4}$$

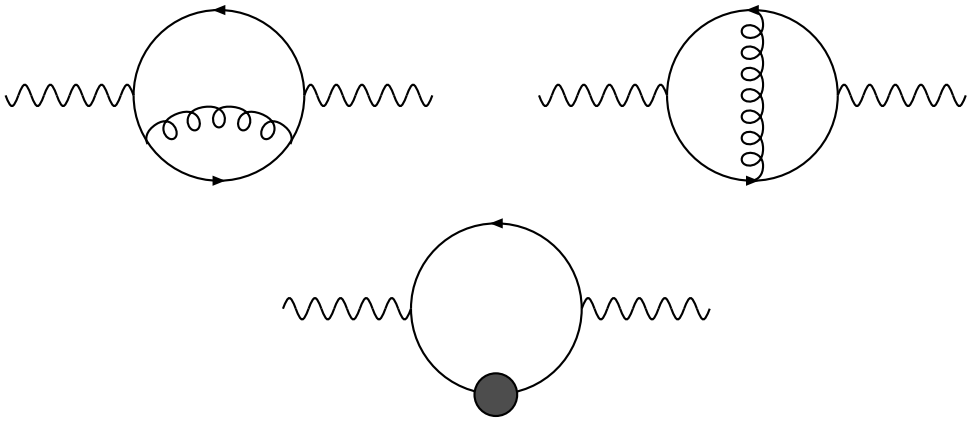

Figure 2: Two loop contribution to the photon self energy. A diagram interchanging the blob in the internal line of the third diagram should also be considered.

where $\mathcal{L}_{\rm ct} = m_{\rm th}^2\phi^2$ is the counter term which should be treated in the same footing as the ϕ^4 term. $\mathcal{L}_{\rm ct}$ has been introduced to avoid thermal corrections at higher order which had already been included in the tree level. With the counter term the Lagrangian remains unchanged, so the effective theory is a mere re-ordering of the perturbative expansion. A similar exercise has to be carried out in gauge theory wherever necessary [56]. The effective action for hot gauge theories have been derived in Refs. [57, 58, 59],whereas the authors of Refs. [60, 61] follow the classical kinetic theory approach for the derivation of the HTL contributions.

The photon emission from Compton and annihilation processes can be calculated from the imaginary parts of the first two diagrams in Fig. (2). Since these processes involve exchange of massless quarks in the t/u channels the rate becomes infrared divergent. One then obtains the hard contribution by introducing a lower cut-off to render the integrals finite. In doing so, some part of the phase space is left out and the rate becomes cut-off dependent. The photon rate from this (soft) part of the phase space is then handled using HTL resummation technique. The application of HTL to hard photon emission rate was first performed in Refs. [15, 16]. For hard photon emission, one of the quark propagators in the photon self energy diagram should be replaced by effective quark propagators (third diagram in Fig. (2)), which consists of the bare propagator and the high temperature limit of one loop corrections [62, 63]. When the hard and the soft contributions are added, the emission rate becomes finite because of the Landau damping of the exchanged quark in the thermal bath and the cut-off scale is canceled. The rate of hard photon emission is then obtained as [15]

$$E\frac{dR_\gamma^{QGP}}{d^3q} = \frac{5}{9}\frac{\alpha\alpha_s}{2\pi^2}T^2\, e^{-E/T}\ln(2.912E/g^2T). \tag{3.5}$$

Recently, the bremsstrahlung contribution to photon emission rate has been computed [17] by evaluating the photon self energy in two loop HTL approximation. The physical processes arising from two loop contribution (Fig. (3)) are the

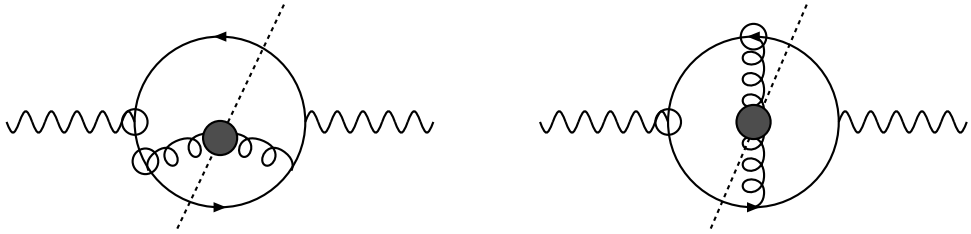

Figure 3: Two loop photon diagram relevant for bremsstrahlung processes. The blob on the gluon (spiral line) indicates effective gluon propagator. The circle on the vertices represents effective vertices.

bremsstrahlung of quarks, antiquarks and quark anti-quark annihilation with scattering in the thermal bath. The rate of photon production due to bremsstrahlung process for a two flavour thermal system with $E > T$ is given by [17]

$$E\frac{dR_\gamma^{QGP}}{d^3q} = \frac{40}{9\pi^5}\,\alpha\alpha_s T^2\, e^{-E/T}\,(J_T - J_L)\ln 2, \tag{3.6}$$

and the rate due to $q - \bar{q}$ annihilation with scattering in the thermal bath is given by,

$$E\frac{dR_\gamma^{QGP}}{d^3q} = \frac{40}{27\pi^5}\,\alpha\alpha_s ET\, e^{-E/T}\,(J_T - J_L)\,, \tag{3.7}$$

where $J_T \approx 4.45$ and $J_L \approx -4.26$. The most important implication of this work is that the two loop contribution is of the same order of magnitude as those evaluated at one loop [15, 16] due to the larger size of the available phase space. In case of soft thermal photon ($E \sim gT$) emission rate, all the vertices and the propagators has to be replaced by the corresponding effective quantities. It has been shown [64, 65] that the result is divergent due to the exchange of massless quarks introduced through the HTL effective vertices itself. However, such collinear singularities for light-like external momentum could be removed with an improved action [59]. It is also shown that such infrared singularities could be removed by including appropriate diagrams and summing over all degenerate initial and final states [66, 67]. As mentioned before we will consider only hard photon emission rate in the present work.

3.2 Photon emission from hot hadronic gas

To evaluate the photon emission rate from a hadronic gas we model the system as consisting of π, ρ, ω and η. The relevant vertices for the reactions $\pi\,\pi \rightarrow \rho\,\gamma$ and $\pi\,\rho \rightarrow \pi\,\gamma$ and the decay $\rho \rightarrow \pi\,\pi\,\gamma$ are obtained from the following Lagrangian:

$$\mathcal{L} = -g_{\rho\pi\pi}\vec{\rho}^\mu \cdot (\vec{\pi} \times \partial_\mu\vec{\pi}) - eJ^\mu A_\mu + \frac{e}{2}F^{\mu\nu}\,(\vec{\rho}_\mu \times \vec{\rho}_\nu)_3, \tag{3.8}$$

where $F_{\mu\nu} = \partial_\mu A_\nu - \partial_\nu A_\mu$, is the Maxwell field tensor and J^μ is the hadronic part of the electromagnetic current given by

$$J^\mu = (\vec{\rho}_\nu \times \vec{B}^{\nu\mu})_3 + (\vec{\pi} \times (\partial^\mu\vec{\pi} + g_{\rho\pi\pi}\vec{\pi} \times \vec{\rho}^\mu))_3, \tag{3.9}$$

with $\vec{B}_{\mu\nu} = \partial_\mu \vec{\rho}_\nu - \partial_\nu \vec{\rho}_\mu - g_{\rho\pi\pi}(\vec{\rho}_\mu \times \vec{\rho}_\nu)$. The invariant amplitudes for all these reactions have been listed in the appendix of Ref. [52].

For the sake of completeness we have also considered the photon production due to the reactions $\pi\,\eta \rightarrow \pi\,\gamma$, $\pi\,\pi \rightarrow \eta\,\gamma$ and the decay $\omega \rightarrow \pi\,\gamma$ using the following interaction [68]:

$$\mathcal{L} = \frac{g_{\rho\rho\eta}}{m_\eta}\,\epsilon_{\mu\nu\alpha\beta}\partial^\mu\rho^\nu\partial^\alpha\rho^\beta\eta + \frac{g_{\omega\rho\pi}}{m_\pi}\,\epsilon_{\mu\nu\alpha\beta}\partial^\mu\omega^\nu\partial^\alpha\rho^\beta\pi + \frac{em_\rho^2}{g_{\rho\pi\pi}}A_\mu\rho^\mu \tag{3.10}$$

The last term in the above Lagrangian is written down on the basis of Vector Meson Dominance (VMD) [69]. The invariant amplitudes for the reactions are given in Ref. [70].

The importance of the role of a_1 as an intermediary meson in the process $\pi\,\rho \rightarrow \pi\,\gamma$ was first emphasized in [71, 72]. Recently it has been shown [73] that the role of intermediary a_1 in this process is less important than thought earlier [71, 72]. The photon production rate obtained in Ref. [74] is similar to that in Ref. [73]. In this article we use the following interaction Lagrangian for the $\pi\rho a_1$ and $\pi a_1\gamma$ vertices [74, 75, 76]:

$$\begin{aligned}\mathcal{L} &= \frac{g^2 f_\pi}{Z_\pi}\Bigg[(2c+Z_\pi)\vec{\pi}\cdot\vec{\rho}_\mu \times \vec{a}^\mu + \frac{1}{2m_{a_1}^2}\vec{\pi}\cdot\vec{B}_{\mu\nu}\times\vec{a}^{\mu\nu} \\ &\quad + \frac{\kappa_6\,Z_\pi}{m_\rho^2}\partial^\mu\vec{\pi}\cdot\vec{B}_{\mu\nu}\times\vec{a}^\nu\Bigg] + \frac{eg\kappa_6 f_\pi}{m_\rho^2}f_{\mu\nu}(\vec{a}^{\mu\nu}\times\vec{\pi})_3\end{aligned} \tag{3.11}$$

where Z_π is the renormalization constant for pion fields, $f_{\mu\nu}$ has been obtained from $\vec{B}_{\mu\nu}$ by using $\rho^0 - \gamma$ mixing ($\rho^0 \rightarrow e f_\mu/g$) [75]. The values of various parameters are $m_{a_1} = 1260$ MeV, $g = 5.04$,$c = -0.12$, $Z_\pi = 0.17$ and $\kappa_6 = 1.25$ [74], chosen to reproduce a_1 width in vacuum. The in-medium mass of the a_1 has been calculated by using Weinberg's sum rule [77].

3.3 Dilepton emission from hot hadronic gas and QGP

In order to express the dilepton emission rate from hadronic matter in terms of the retarded current correlation function we use Eq. 2.31 and Eq. 2.40 to obtain,

$$\frac{dR}{d^4q} = -\frac{\alpha}{12\pi^4\,q^2}(1+\frac{2m^2}{q^2})\sqrt{1-\frac{4m^2}{q^2}}\mathrm{Im}W_\mu^{R\mu}\,f_{BE}(q_0) \tag{3.12}$$

The parameterized form of the electromagnetic current correlation function in the ρ and ω channels will be discussed in detail in Sec.5.2. Now instead of using the current correlation function directly in the above equation one can use vector meson dominance (VMD) to obtain the dilepton yield from ($\pi^+\pi^- \rightarrow e^+e^-$) which is known to be the most dominant source of dilepton production. In the low mass region one should also add the contributions from the decay of vector mesons such as ρ and ω. This is usually done in the literature. In order to make a comparative

study we state briefly how the emission rate from pion annihilation can be derived from Eq. 3.12. VMD relates the hadronic electromagnetic current to the vector meson field through field current identity as

$$J^h_\mu = -\sum_V \frac{e}{g_V} m_V^2 V_\mu \tag{3.13}$$

where, $V = \rho, \omega, \phi$. We shall keep only rho meson in the following. The electromagnetic current correlator can then be expressed in terms of the propagator of the vector particle in the following way:

$$\mathrm{Im}W^R_{\mu\nu} = -\frac{e^2 m_\rho^4}{g_\rho^2} \mathrm{Im}D^{\rho R}_{\mu\nu} \tag{3.14}$$

where

$$\begin{aligned} \mathrm{Im}D^{\rho R}_{\mu\nu} &= A_{\mu\nu}\left[\frac{\mathrm{Im}\Pi_T^{\rho R}}{(q^2 - m_\rho^2 + \mathrm{Re}\Pi_T^{\rho R})^2 + [\mathrm{Im}\Pi_T^{\rho R}]^2}\right] \\ &\quad + B_{\mu\nu}\left[\frac{\mathrm{Im}\Pi_L^{\rho R}}{(q^2 - m_\rho^2 + \mathrm{Re}\Pi_L^{\rho R})^2 + [\mathrm{Im}\Pi_L^{\rho R}]^2}\right]. \end{aligned} \tag{3.15}$$

In the approximation $\Pi_T^{\rho R} = \Pi_L^{\rho R} = \Pi^{\rho R}$ we can define the rho spectral function in VMD as

$$\mathrm{Im}W^R_L = \frac{e^2 m_\rho^4}{g_\rho^2 q^2}\left[\frac{\mathrm{Im}\Pi^{\rho R}}{(q^2 - m_\rho^2 + \mathrm{Re}\Pi^{\rho R})^2 + [\mathrm{Im}\Pi^{\rho R}]^2}\right]. \tag{3.16}$$

Using Eq. 3.12 we obtain the dilepton rate from pion annihilation as

$$\begin{aligned} \frac{dR}{dM} &= \frac{2\alpha^2}{\pi^2}\frac{m_\rho^4}{g_\rho^2}\frac{1}{M}\left(1 + \frac{2m^2}{M^2}\right)\sqrt{1 - \frac{4m^2}{M^2}} \\ &\times \int e^{-M_T \cosh y/T} M_T dM_T dy \left[\frac{\mathrm{Im}\Pi^{\rho R}}{(M^2 - m_\rho^2 + \mathrm{Re}\Pi^{\rho R})^2 + [\mathrm{Im}\Pi^{\rho R}]^2}\right] \end{aligned} \tag{3.17}$$

in the Boltzmann approximation. This on simplification gives

$$\frac{dR}{dM} = \frac{\sigma(M)}{(2\pi)^4} M^4 T \sum_n \frac{K_1(nM/T)}{n}(1 - 4m_\pi^2/M^2), \tag{3.18}$$

where K_1 is the modified Bessel function, and M is the invariant mass of the lepton pair and $\sigma(M)$ is the cross-section for the pion annihilation given by

$$\sigma(M) = \frac{4\,\pi\,\alpha^2}{3\,M^2}\sqrt{1 - 4m_\pi^2/M^2}\,\sqrt{1 - 4m^2/M^2}\,(1 + 2m^2/M^2)\,|F_\pi(M)|^2, \tag{3.19}$$

where

$$|F_\pi(M)|^2 = \frac{m_\rho^4}{(M^2 - m_\rho^2 + \mathrm{Re}\Pi^{\rho R})^2 + (\mathrm{Im}\Pi^{\rho R})^2} \tag{3.20}$$

In the same way, the invariant mass distribution of lepton pairs from the vector meson decays is obtained using Eq. 2.38, as

$$\begin{aligned}\frac{dR}{dM} &= \frac{2J+1}{\pi^2}\,M^2T\sum_n\frac{K_1(nM/T)}{n} \\ &\times\frac{M\Gamma_{\rm tot}/\pi}{(M^2-m_V^2+{\rm Re}\Pi^{\rho R})^2+M^2\Gamma_{\rm tot}^2}M\Gamma^{\rm vac}_{V\to e^+e^-},\end{aligned} \tag{3.21}$$

where $\Gamma_{\rm tot}$ is the width of the vector meson in the medium and $\Gamma^{\rm vac}_{V\to e^+e^-}$ is the partial width for the leptonic decay mode for the off-shell vector mesons in vacuum given by

$$\Gamma^{\rm vac}_{V\to e^+e^-} = \frac{4\pi\alpha^2M}{3g_\rho^2}\sqrt{1-4m^2/M^2}\,(1+2m^2/M^2) \tag{3.22}$$

where m is the mass of the electron.

We have considered quark anti-quark annihilation for the evaluation of dilepton emission rate from QGP [8]. The dilepton rate is given by

$$\frac{dR}{dM} = \frac{\sigma_{q\bar q}(M)}{(2\pi)^4}\,M^4\,T\sum_n\frac{K_1(nM/T)}{n} \tag{3.23}$$

with the cross section

$$\sigma_{q\bar q\to e^+e^-} = \frac{80\pi}{9}\frac{\alpha^2}{M^2}\sqrt{\left(1-\frac{4m^2}{M^2}\right)}\left(1+\frac{2m^2}{M^2}\right). \tag{3.24}$$

4 Hadronic properties in nuclear matter at finite temperature

As emphasized earlier, the photon and dilepton emission rates are related to the imaginary part of the photon self energy in the medium. In this section we will study the in-medium modifications of the particles appearing in the internal thermal loop of the photon self energy diagram. Here the hadronic medium consists of mesons and baryons at a finite temperature. Due to the interactions with real and virtual excitations, the properties of these hadrons are expected to get modified. As a result the propagators appearing in the photon self energy undergo modifications. The subject of the present section is to discuss how one incorporates these changes in the framework of Thermal Field Theory [37, 40, 78, 79].

Let us start with some general considerations in the real time formalism. The Greens functions in the imaginary or Matsubara formalism can be obtained by proper analytic continuation [80, 81].

The free propagator of a scalar field ϕ in vacuum is defined as

$$\begin{aligned}i\bar\Delta^0(p) &= \int d^4x\,e^{-ipx}\langle[T\{\phi(x)\phi(0)\}]\rangle_0 \\ &= \frac{i}{p^2-m^2+i\epsilon}\end{aligned} \tag{4.1}$$

For a fermion field, this can be expressed as

$$i\bar{G}^0(p)_{\alpha\beta} = (\not{p} + m)_{\alpha\beta} i\bar{\Delta}^0, \tag{4.2}$$

and for a massive vector particle as

$$i\bar{D}^0(p)^{\mu\nu} = (-g^{\mu\nu} + p^\mu p^\nu/m^2) i\bar{\Delta}^0. \tag{4.3}$$

The interacting propagator is related to the bare(non-interacting) propagator defined above through the Dyson-Schwinger Equation.

$$\bar{\Delta} = \bar{\Delta}_0 + \bar{\Delta}_0 \Pi \bar{\Delta} \tag{4.4}$$

Where, Π is the self energy of the particle due to interactions.

Let us now study the situation in a medium at finite temperature (and density) for the fermion fields. In the real time formalism the non-interacting finite temperature propagator assumes a matrix structure because of doubling of the degrees of freedom [40].

$$\begin{aligned} i\mathbf{G}^{\mathbf{0}}_{\alpha\beta} &= \begin{bmatrix} iG^{0(11)}_{\alpha\beta}(p) & iG^{0(12)}_{\alpha\beta}(p) \\ iG^{0(21)}_{\alpha\beta}(p) & iG^{0(22)}_{\alpha\beta}(p) \end{bmatrix} \\ &= \begin{bmatrix} \int d^4x\, e^{ip\cdot x} \langle T\{\psi_\alpha(x)\psi_\beta(0)\}\rangle^0_T & \int d^4x\, e^{ip\cdot x} \langle \{\psi_\alpha(0)\psi_\beta(x)\}\rangle^0_T \\ \int d^4x\, e^{ip\cdot x} \langle \{\psi_\alpha(x)\psi_\beta(0)\}\rangle^0_T & \int d^4x\, e^{ip\cdot x} \langle \bar{T}\{\psi_\alpha(x)\psi_\beta(0)\}\rangle^0_T \end{bmatrix} \end{aligned} \tag{4.5}$$

The elements of $\mathbf{G}^{\mathbf{0}}_{\alpha\beta}$ (in momentum space) are,

$$\begin{aligned} G^{0(11)}_{\alpha\beta}(p) &= (\not{p} + m)_{\alpha\beta} \left[\frac{1}{p^2 - m^2 + i\epsilon} + 2\pi i \delta(p^2 - m^2) \eta(p.u) \right] \\ G^{0(12)}_{\alpha\beta}(p) &= 2\pi i (\not{p} + m)_{\alpha\beta} \delta(p^2 - m^2) [\eta(p.u) - \theta(-p.u)] \\ G^{0(21)}_{\alpha\beta}(p) &= 2\pi i (\not{p} + m)_{\alpha\beta} \delta(p^2 - m^2) [\eta(p.u) - \theta(p.u)] \\ G^{0(22)}_{\alpha\beta}(p) &= (\not{p} + m)_{\alpha\beta} \left[\frac{-1}{p^2 - m^2 - i\epsilon} + 2\pi i \delta(p^2 - m^2) \eta(p.u) \right] \end{aligned} \tag{4.6}$$

where, $\eta(p.u) = \theta(p.u) f_{FD}(x) + \theta(-p.u) f_{FD}(-x)$, $f_{FD} = [e^x + 1]^{-1}$ with $x = \beta(p \cdot u - \mu)$ and u^μ is the four velocity of the thermal bath. It is important to note that the real time propagator consists of two parts - one corresponding to the vacuum, describing the exchange of virtual particle and the other, the temperature dependent part, describing the participation of real (on-shell) particles present in the thermal bath in the emission and absorption processes. The temperature dependent part does not change the ultra-violet behaviour of the theory as it contains on-shell contributions which has a natural cut-off due to the Boltzmann factor. Therefore, the zero temperature counter term is adequate for the renormalization of the theory.

However, the infra-red problem becomes more severe at finite temperature [37, 82, 83].

The interacting propagator at finite temperature is again obtained from the Dyson equation. In this case it will be a matrix equation:

$$\mathbf{G} = \mathbf{G^0} + \mathbf{G^0 \Sigma G}, \tag{4.7}$$

where $\mathbf{\Sigma}$ is a 2×2 matrix of self energies. Though all the four components are required for the consistency of the theory, only $G^{(11)}_{\alpha\beta}(p)$ is physically relevant in our case. We will henceforth denote this as $G(p)$. For the same reason we will concern ourselves with the $(1,1)$ component of $\mathbf{\Sigma}$. Its real part affects the dispersion relation of the particle in the medium. The displaced pole position of the effective propagator in the rest frame of the propagating particle (i.e. where the three momentum of the particle is zero) gives the effective mass of the particle in the medium.

The interacting propagators at finite temperature for scalar and vector fields can be described along the same lines. In the following we will discuss the case of vector mesons in some detail. In general the matrix equation for the interacting propagator can be written in diagonal form. Diagonalization can be performed in various ways [84] by properly choosing the transformations. The diagonal element satisfies Dyson equation

$$D^{-1}_{\mu\nu} = (D^0_{\mu\nu})^{-1} - \Pi_{\mu\nu}, \tag{4.8}$$

where

$$D^0_{\mu\nu} = \frac{-g_{\mu\nu} + p_\mu p_\nu/m^2}{p^2 - m^2 + i\epsilon} \tag{4.9}$$

is the free-space (bare) propagator; $p^\mu = (\omega, \mathbf{p})$ is the four-momentum of the propagating particle and m is the bare mass of the vector meson. $\Pi_{\mu\nu}$ is the self energy of the vector meson given by

$$\Pi^{\mu\nu} = \Pi^{\mu\nu}_{\rm vac} + \Pi^{\mu\nu}_{\rm med}, \tag{4.10}$$

where

$$\Pi^{\mu\nu}_{\rm vac} = (g^{\mu\nu} - \frac{p^\mu p^\nu}{p^2})\,\Pi_{\rm vac}(p^2), \tag{4.11}$$

is the vacuum contribution to the self energy. In a thermal bath moving with four-velocity u^μ $\Pi^{\mu\nu}_{\rm med}$ has transverse and longitudinal components [40]:

$$\Pi^{\mu\nu}_{\rm med}(\omega, \mathbf{p}) = A^{\mu\nu}\Pi_{T,\rm med} + B^{\mu\nu}\Pi_{L,\rm med}. \tag{4.12}$$

$A^{\mu\nu}$ and $B^{\mu\nu}$ are the transverse and longitudinal projection tensors given by

$$A^{\mu\nu} = \frac{1}{p^2 - \omega^2}\left[(p^2 - \omega^2)(g^{\mu\nu} - u^\mu u^\nu)\ - p^\mu p^\nu - \omega^2 u^\mu u^\nu + \omega(u^\mu p^\nu + p^\mu u^\nu)\right], \tag{4.13}$$

and

$$B^{\mu\nu} = \frac{1}{p^2(p^2 - \omega^2)}\left[\,\omega^2 p^\mu p^\nu + p^4 u^\mu u^\nu - \omega p^2(u^\mu p^\nu + p^\mu u^\nu)\right], \tag{4.14}$$

which obey the relation

$$A^{\mu\nu} + B^{\mu\nu} = g^{\mu\nu} - \frac{p^\mu p^\nu}{p^2}. \tag{4.15}$$

Using Eqs. (4.8-4.15) the effective propagator becomes

$$D_{\mu\nu} = -\frac{A_{\mu\nu}}{p^2 - m^2 + \Pi_T} - \frac{B_{\mu\nu}}{p^2 - m^2 + \Pi_L} + \frac{p_\mu p_\nu}{p^4}, \tag{4.16}$$

where

$$\Pi_{T(L)} = \Pi_{T(L),\mathrm{med}} + \Pi_{\mathrm{vac}}. \tag{4.17}$$

4.1 The Walecka model - Nucleon Mass

Before discussing the vector meson masses in the medium let us see how the nucleon properties are modified in matter at finite temperature. Nuclear matter is studied using the Quantum Hadrodynamics (QHD) model [29] in which the nucleons interact through the exchange of scalar sigma and the vector omega mesons. The interaction in this model is described by the Lagrangian

$$\mathcal{L}_I = -g_v\, \bar{N}\gamma_\mu\, N\, \omega^\mu + g_s\, \bar{N}\, \sigma\, N, \tag{4.18}$$

where $N(x)$, $\sigma(x)$, and $\omega(x)$ are the nucleon, sigma, and omega mesons fields respectively. The $\sigma(\omega)$ field couples to the nucleon scalar (vector) current with the coupling constant $g_s(g_v)$ which will be specified later.

The free nucleon propagator at finite temperature and density is given by

$$\begin{aligned} G^0(k) &= G^{0(11)}(k) \\ &= (\not{k} + M)\left[\frac{1}{k^2 - M^2 + i\epsilon} + 2\pi i\delta(k^2 - M^2)\eta(k.u)\right] \\ &= G^0_F(k) + G^0_D(k), \end{aligned} \tag{4.19}$$

where the first term (G^0_F) describes the free propagation of nucleon-antinucleon pairs and the second term (G^0_D) allows for the on-shell propagation of particle-hole pairs. M in the above equation is the free nucleon mass.

The effective mass of the nucleon in matter at finite temperature in the presence of interaction described by Eq. 4.18 will appear as a pole of the effective nucleon propagators given by Eq. 4.7. In the Relativistic Hartree Approximation (RHA) [29, 30] one obtains the effective propagator by summing up scalar and vector tadpole diagrams self-consistently i.e. by using the interacting propagators to determine the self energy. The effective propagator also called Hartree propagator is given by (see Fig. (4))

$$G^H(k) = G^0(k) + G^0(k)\Sigma^H(k)G^H(k) \tag{4.20}$$

where $\Sigma^H(k)$ is the nucleon self energy which contains contributions from both scalar (Σ_s) and vector (Σ^μ_v) tadpole diagrams [29, 30] and is given by

$$\Sigma^H = \Sigma^H_s - \gamma^\mu \Sigma^H_{\mu v}, \tag{4.21}$$

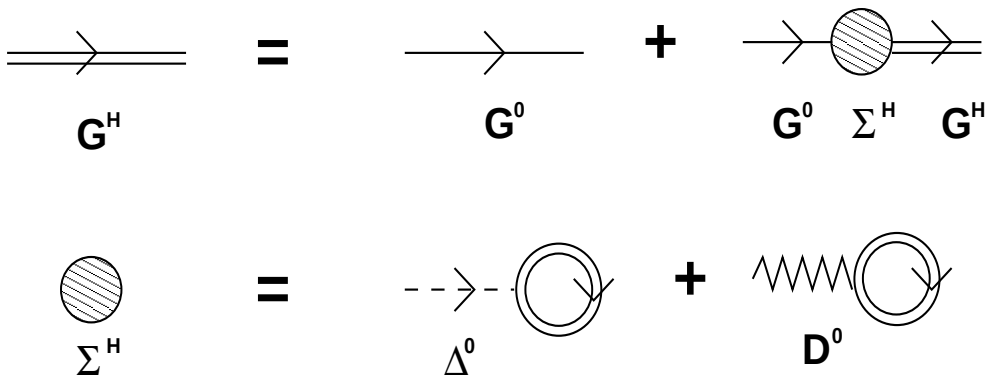

Figure 4: Diagrammatic representation of Dyson-Schwinger equation for nucleons in RHA

where

$$\Sigma_s^H = i\frac{g_s^2}{m_s^2}\int \frac{d^4p}{(2\pi)^4}\,\mathrm{Tr}[G^H(p)] \tag{4.22}$$

and,

$$\Sigma_{\mu v}^H = i\frac{g_v^2}{m_v^2}\int \frac{d^4p}{(2\pi)^4}\,\mathrm{Tr}[\gamma_\mu\, G^H(p)] \tag{4.23}$$

Here, m_s (m_v) is the mass of the neutral scalar (vector) meson. The solution of Eq. 4.20 now reads,

$$\begin{aligned} G^H(p) &= (\not{\bar{p}} + M^*)\left[\frac{1}{\bar{p}^2 - M^{*2} + i\epsilon} + 2\pi i\delta(\bar{p}^2 - M^{*2})\eta(\bar{p}.u)\right] \\ &= G_F^H(p) + G_D^H(p) \end{aligned} \tag{4.24}$$

One observes that the pole structure of the full nucleon propagator in RHA resembles that of the non-interacting propagator with shifted mass and four-momentum i.e. $\bar{p} = p + \Sigma_v^H$ amd $M^* = M + \Sigma_s^H$. Using G_D^H in place of the full Hartree propagator in Eqs. 4.22 and 4.23 defines the Mean Field Theory (MFT) values of the self energies. This is equivalent to solving the meson field equations with the replacement of the meson field operators by their expectation values which become classical fields i.e. $\sigma \to \langle\sigma\rangle$ and $\omega \to \langle\omega\rangle$. This yields $\langle\sigma\rangle = g_s\,\rho_s/m_s^2$ and $\langle\omega^\mu\rangle = g_v\,\delta^{\mu 0}\rho_B/m_v^2$ which indicate that the nuclear ground state contains scalar and vector meson condensates generated by baryon sources. The spatial part of the omega condensate vanishes due to rotational symmetry in infinite nuclear medium. These condensates are related to the scalar and vector self energies generated by summing tadpole diagrams in QHD as, $\Sigma_s = -g_s\langle\sigma\rangle$ and $\Sigma_v^0 = -g_v\langle\omega^0\rangle$. The mean field approximation is thus to neglect the fluctuations in the meson fields which themselves are generated by the nucleons.

RHA is obtained when one includes the vacuum fluctuation corrections to the MFT results. This amounts to the inclusion of the Dirac part of the propagator G_F^H in the calculation of the self energies. Summing over the vacuum tadpoles

results in a sum over all occupied states in the negative energy sea of nucleons. Vacuum or quantum fluctuations, as these are called forms an essential ingredient in a relativistic theory of many particle systems. Since there are infinite number of negative energy states in the vacuum one expects that the vacuum contribution to the self energy is infinite.

Let us now find the Hartree self energy of the nucleon with the full nucleon propagator which consists a medium and a vacuum part. The vector part of the self energy is obtained from Eq. 4.23 as

$$\Sigma_v^{H\mu} = 8i\frac{g_v^2}{m_v^2}\int \frac{d^4p}{(2\pi)^4}\,\frac{\bar{p}^\mu}{\bar{p}^2 - M^{*2} + i\epsilon} - \frac{g_v^2}{m_v^2}\delta^{\mu 0}\rho_B. \tag{4.25}$$

The first term of this equation appears to be divergent. The usual procedure is to regularize the integral in n dimensions by dimensional regularization to render the integral finite. One can then shift the integration variable from p to $\bar{p}$. The resulting integral vanishes by symmetric integration. The vector self energy then reduces to $\Sigma_v^{H\mu} = -g_v^2\delta^{\mu 0}\rho_B/m_v^2$ and thus gives rise to a an effective chemical potential, $\mu^* = \mu - g_v^2\,\rho_B/m_v^2$. The scalar part of the self energy follows from Eq. 4.22:

$$\Sigma_s^H = 8i\frac{g_s^2}{m_s^2}\int \frac{d^4p}{(2\pi)^4}\,\frac{M^{*2}}{\bar{p}^2 - M^{*2} + i\epsilon} - \frac{4g_s^2}{m_s^2}\int \frac{d^3p}{(2\pi)^3}\frac{M^*}{E^*}\,\Big[\,f_{BE}(\mu^*,T) + \bar{f}_{BE}(\mu^*,T)\Big] \tag{4.26}$$

where

$$\begin{aligned} f_{BE}(\mu^*,T) &= \frac{1}{\exp[(E^*-\mu^*)/T]+1} \\ \bar{f}_{BE}(\mu^*,T) &= \frac{1}{\exp[(E^*+\mu^*)/T]+1} \\ E^* &= \sqrt{(\vec{p}^2 + M^{*2})} \end{aligned} \tag{4.27}$$

Here ρ_B is the baryon density (in the present work we will take $\rho_B = 0$) of the medium and is given by

$$\rho_B = \frac{4}{(2\pi)^3}\int d^3p\,[f_{BE}(\mu^*,T) - \bar{f}_{BE}(\mu^*,T)]. \tag{4.28}$$

The first term in Eq. 4.26, to be denoted by $\Sigma_s^{(1)}$, represents the contribution to the scalar self energy from the filled Dirac sea and is ultraviolet divergent. We will now proceed to renormalize this divergent contribution. The first step is to isolate the divergences through dimensional regularization. This gives

$$\begin{aligned} \Sigma_s^{(1)} &= -\frac{g_s^2}{m_s^2}\frac{\Gamma(2-n/2)}{2\pi^2}M^{*3} \\ &= -\frac{g_s^2}{m_s^2}\frac{\Gamma(2-n/2)}{2\pi^2}(M^3 + 3M^2\Sigma_s^H + 3M\Sigma_s^{H\,2} + \Sigma_s^{H\,3}) \end{aligned} \tag{4.29}$$

The divergence in $\Sigma_s^{(1)}$ now appears in the pole of the Γ-function for physical dimension $n = 4$. The counter terms needed to remove the divergent contributions from the loop corrections to the measurable amplitudes are

$$\mathcal{L}_{CT} = \sum_{n=1}^{4} \alpha_n \, \sigma^n / n!. \tag{4.30}$$

Including the contributions from the counter terms the renormalized self energy becomes

$$\Sigma_s^{(1)ren} = \Sigma_s^{(1)} + \Sigma_s^{CTC}, \tag{4.31}$$

where

$$\Sigma_s^{CTC} = \sum_{n=0}^{3} \frac{1}{n!} \left(\frac{-g_s}{m_s^2} \right) \left(\frac{-\Sigma_s^H}{g_s} \right)^n \alpha_{n+1}. \tag{4.32}$$

The coefficients (α) are fixed by defining a set of renormalization conditions. Since the scalar density $\langle \bar{\psi}\psi \rangle$ is not a conserved quantity the tadpole diagrams appear in the self energy. The tadpole contribution must vanish in normal vacuum (free space) i.e. $\langle \sigma \rangle_0 = 0$. This is ensured by the term $\alpha_1 \sigma$ in $\mathcal{L}_{CT}$. $\alpha_2 \sigma^2$ is the meson mass counter term which ensures that m_s is the physical (measured) mass. Since the original Lagrangian of QHD [29] does not contain σ^3 and σ^4 terms, at the tree level, three and four point meson amplitudes must vanish. The last two counter terms in Eq. 4.30 are chosen to maintain this condition at zero external momenta for the sigma meson when nucleon loop corrections are included. We thus have

$$\alpha_n = -i(-g_s)^n (n-1)! \int \frac{d^4p}{(2\pi)^4} \mathrm{Tr}[G_F^0(p)^n]. \tag{4.33}$$

Consequently the effective nucleon mass reads

$$\begin{aligned} \Sigma_s^H &= M^* - M \\ &= -\frac{4g_s^2}{m_s^2} \int \frac{d^3p}{(2\pi)^3} \frac{M^*}{E^*} \Big[f_{BE}(\mu^*, T) + \bar{f}_{BE}(\mu^*, T) \Big] \\ &+ \frac{g_s^2}{m_s^2} \frac{1}{\pi^2} \Big[M^{*3} \ln \left(\frac{M^*}{M} \right) - M^2 (M^* - M) \\ &- \frac{5}{2} M (M^* - M)^2 - \frac{11}{6} (M^* - M)^3 \Big]. \end{aligned} \tag{4.34}$$

The solution of this equation gives the effective nucleon mass M^* as a function of temperature and baryon density. At zero baryon density it can be parametrised as

$$M^* = M \left[1 - 0.0264 \left(\frac{T}{0.16} \right)^{8.94} \right]. \tag{4.35}$$

where T is in GeV.

4.2 The vector meson mass

In a medium meson properties get modified due to its coupling to nuclear excitations. This modification is contained in the meson self energy which appears in the Dyson-Schwinger equation for the effective propagator in the medium. The interaction vertices are provided by the Lagrangian

$$\mathcal{L}_{VNN} = g_{VNN}\left(\bar{N}\gamma_\mu\tau^a N V_a^\mu - \frac{\kappa_V}{2M}\bar{N}\sigma_{\mu\nu}\tau^a N\partial^\nu V_a^\mu\right), \tag{4.36}$$

where $V_a^\mu = \{\omega^\mu, \vec{\rho}^\mu\}$, M is the free nucleon mass, N is the nucleon field and $\tau_a = \{1, \vec{\tau}\}$.

The lowest order contribution to the vector meson self energy is expressed in terms of the self-consistent nucleon propagator described above Eq. 4.24. This is given by

$$\Pi^{\mu\nu}(k) = -2ig_v^2\int\frac{d^4p}{(2\pi)^4}\mathrm{Tr}\left[\Gamma^\mu(k)\,G^H(p)\Gamma^\nu(-k)\,G^H(p+k)\right], \tag{4.37}$$

where Γ^μ represents the meson-nucleon vertex function obtained from eq.(4.36) and is given by

$$\begin{aligned}\Gamma^\mu(k) &= \gamma^\mu; && \text{for } \omega\\ \Gamma^\mu(k) &= \gamma^\mu + i\frac{\kappa_\rho}{2M}\sigma^{\mu\alpha}k_\alpha; && \text{for } \rho\end{aligned} \tag{4.38}$$

The vector meson self energy can be written as a sum of two parts

$$\Pi^{\mu\nu}(k) = \Pi_F^{\mu\nu}(k) + \Pi_D^{\mu\nu}(k), \tag{4.39}$$

where

$$\begin{aligned}\Pi_F^{\mu\nu}(k) &= -2ig_v^2\int\frac{d^4p}{(2\pi)^4}\mathrm{Tr}\left[\Gamma^\mu(k)\,G_F^H(p)\Gamma^\nu(-k)\,G_F^H(p+k)\right]\\ \Pi_D^{\mu\nu}(k) &= -2ig_v^2\int\frac{d^4p}{(2\pi)^4}\mathrm{Tr}\left[\Gamma^\mu(k)\,G_F^H(p)\Gamma^\nu(-k)\,G_D^H(p+k)\right.\\ &\quad +\Gamma^\mu(k)\,G_D^H(p)\Gamma^\nu(-k)\,G_F^H(p+k)\\ &\quad \left.+\,\Gamma^\mu(k)\,G_D^H(p)\Gamma^\nu(-k)\,G_D^H(p+k)\right].\end{aligned} \tag{4.40}$$

$\Pi_F^{\mu\nu}$ is the vacuum polarization. This is a bilinear function of G_F^H and hence describes the correction to the meson propagators due to coupling to $N\bar{N}$ excitations. The $N\bar{N}$ pairs can be excited only if the four-momentum carried by the mesons is in the time-like region ($k^2 > 0$). Hence the shift in the mass of the vector mesons due to vacuum polarization is caused by processes like $V \to N\bar{N} \to V$ where N represents nucleons in the modified Dirac sea having an effective mass M^*, smaller than what it would be in free space. We have seen that $\Pi_F^{\mu\nu}$ causes a substantial negative shift in the masses of vector mesons.

¿From Eq. 4.40 we have

$$\Pi_F^{\mu\nu}(k) = -2ig_{VNN}^2 \int \frac{d^4p}{(2\pi)^4} \frac{\mathrm{Tr}[\Gamma^\mu(\not{p}+M^*)\Gamma^\nu(\not{p}+\not{k}+M^*)]}{(p^2-M^{*2})[(p+k)^2-M^{*2}]}. \tag{4.41}$$

¿From naive power counting it can be seen that this part of the self energy is ultraviolet divergent and has to be renormalized. A few comments about renormalizability of the interaction given by Eq. 4.36 is in order here. At very large momenta the propagator for massless boson $\sim O(k^{-2})$, whereas for massive vector bosons it goes as $\sim O(1)$. This poses severe problems to the renormalizability of the theory with massive vector bosons. However, in a gauge theory with spontaneous symmetry breaking the vector gauge bosons acquire mass in such a way that the renormalizability of the theory is always preserved. The theory which involves neutral massive vector bosons coupled to a conserved current is also renormalizable. This is because in a physical process the propagator $\bar{D}_0^{\mu\nu} = (-g^{\mu\nu} + p^\mu p^\nu/m^2)/(p^2 - m^2 + i\epsilon)$ appears between two conserved currents J_μ and J_ν and the offending term $p^\mu p^\nu/m^2$ does not contribute because of current conservation ($p_\mu J^\mu = 0$), making the theory renormalizable. This is the case for the omega meson which we shall consider first (see Ref. [85, 86]). The counter term required in this case is

$$\mathcal{L}_{VNN}^{CT} = -\frac{1}{4}\zeta V^{\mu\nu} V_{\mu\nu}. \tag{4.42}$$

We use dimensional regularization to separate the divergent and the finite parts. The divergences now appear as a pole in the gamma function at the physical dimension $n = 4$. The renormalized vacuum polarization tensor for the omega is then given by

$$\Pi_F^{\mu\nu}(k) = (g^{\mu\nu} - k^\mu k^\nu/k^2)\Pi_F^{ren}(k^2), \tag{4.43}$$

where

$$\begin{aligned} \Pi_F^{ren}(k^2) &= \frac{g_{\omega NN}^2}{\pi^2}\left\{\Gamma(2-n/2)\int_0^1 dz\, z(1-z)\right. \\ &\quad \left. - \int_0^1 dz\, z(1-z)\ln[M^{*2} - k^2 z(1-z)]\right\} - \zeta \end{aligned} \tag{4.44}$$

in which the counter term contribution

$$\Pi_F^{\mu\nu CTC} = -\zeta(g^{\mu\nu} - k^\mu k^\nu/k^2) \tag{4.45}$$

has been included. ζ is now determined by the renormalization condition

$$\Pi_F^{ren}(k^2)|_{M^*\to M} = 0. \tag{4.46}$$

Finally, we arrive at

$$\begin{aligned} \Pi_F^{\omega}(k^2) &= \frac{1}{3}\mathrm{Re}(\Pi_F^{ren})_\mu^\mu \\ &= -\frac{g_{\omega NN}^2 k^2}{\pi^2}\int_0^1 dz\, z(1-z)\ln\left[\frac{M^{*2} - k^2 z(1-z)}{M^2 - k^2 z(1-z)}\right]. \end{aligned} \tag{4.47}$$

Renormalization of the vacuum self energy for the rho meson presents additional problems because of the tensor interaction. A phenomenological subtraction procedure, as described in Refs. [87, 88] is used to arrive at the following expressions:

$$\Pi_F^{\rho}(k^2) = -\frac{g_{\rho NN}^2}{\pi^2} k^2 \left[I_1 + M^* \frac{\kappa_\rho}{2M} I_2 + \frac{1}{2} \left(\frac{\kappa_\rho}{2M}\right)^2 (k^2 I_1 + M^{*2} I_2) \right], \tag{4.48}$$

where

$$I_1 = \int_0^1 dz\, z(1-z)\, \ln\left[\frac{M^{*2} - k^2\, z(1-z)}{M^2 - k^2\, z(1-z)} \right], \tag{4.49}$$

$$I_2 = \int_0^1 dz\, \ln\left[\frac{M^{*2} - k^2\, z(1-z)}{M^2 - k^2\, z(1-z)} \right]. \tag{4.50}$$

The medium dependent part of the polarization, $\Pi_D^{\mu\nu}$, describes the coupling of the vector mesons to particle-hole excitations. It contains at least one on-shell nucleon propagator which provides a natural ultraviolet cutoff in the loop momenta. This part of the self energy leads to an increased effective mass of the vector mesons in the medium.

The change in the hadronic mass in the medium can be understood from the following phenomenological arguments [89]. Consider the propagation of a vector meson in a nuclear medium. The attenuation of the amplitude at a distance z, in a fermi gas approximation, is given by $e^{-n\sigma z}$, where n is the density of nucleons and σ is the meson-nucleon interaction cross section. The optical theorem relates σ to the imaginary part of the forward scattering amplitude; $\sigma = 4\pi \mathrm{Im} f(E)/k$. It then follows that the meson wave function $\psi \sim \exp[2\pi i n z f(E)/k]$. In terms of an effective mass ($m_{\rm eff} = m + \Delta m$), the propagation can also be described by $\psi \sim \exp[i\sqrt{E^2 - m_{\rm eff}^2}\, z]$. Comparing the arguments of the exponential we get

$$\Delta m = -\frac{2\pi n k}{m} \mathrm{Re} f(E). \tag{4.51}$$

This relation clearly shows that the enhancement or reduction of hadronic masses depends on the sign of $Ref(E)$.

In a hot and dense medium because of Lorentz invariance and current conservation the general structure of the polarization tensor takes the form

$$\Pi^{\mu\nu} = \Pi_T(k_0, |\vec{k}|) A^{\mu\nu} + \Pi_L(k_0, |\vec{k}|) B^{\mu\nu} \tag{4.52}$$

where the two Lorentz invariant functions Π_T and Π_L are obtained by contraction:

$$\begin{aligned} \Pi_L &= -\frac{k^2}{|\vec{k}|^2} u^\mu u^\nu \Pi_{\mu\nu} \\ \Pi_T &= \frac{1}{2}(\Pi_\mu^\mu - \Pi_L) \end{aligned} \tag{4.53}$$

In the case of the vector meson interacting with real particle-hole excitations in the nuclear medium these are given by

$$\begin{aligned}\Pi^D_{\mu\nu} &= -2ig^2_{VNN}\int\frac{d^4p}{(2\pi)^4}\,\mathrm{Tr}\Big[\,\Gamma^\mu(k)G_F(p)\Gamma^\nu(-k)G_D(p+k)+(F\leftrightarrow D)\Big]\\ &= (\Pi^D_v+\Pi^D_{vt}+\Pi^D_t)_{\mu\nu}\end{aligned}\tag{4.54}$$

with

$$\begin{aligned}(\Pi^D_v)^\mu_\mu &= \frac{g^2_{VNN}}{2\pi^2}\frac{1}{|\vec{k}|}\int\frac{pdp}{\omega_p}\,\Bigg[(k^2+2M^{*2})\ln\left\{\frac{(k^2+2|\vec{p}||\vec{k}|)^2-4k_0^2\omega_p^2}{(k^2-2|\vec{p}||\vec{k}|)^2-4k_0^2\omega_p^2}\right\}\\ &\quad-\,8|\vec{p}||\vec{k}|\Bigg]\,\Big[\,f_{BE}(\mu^*,T)+\bar{f}_{BE}(\mu^*,T)\Big]\end{aligned}\tag{4.55}$$

$$\begin{aligned}(\Pi^D_{vt})^\mu_\mu &= \frac{3g^2_{VNN}}{\pi^2}M^*\left(\frac{\kappa_V}{2M}\right)\frac{k^2}{|\vec{k}|}\int\frac{pdp}{\omega_p}\,\ln\left\{\frac{(k^2+2|\vec{p}||\vec{k}|)^2-4k_0^2\omega_p^2}{(k^2-2|\vec{p}||\vec{k}|)^2-4k_0^2\omega_p^2}\right\}\\ &\quad\times\Big[\,f_{BE}(\mu^*,T)+\bar{f}_{BE}(\mu^*,T)\Big]\end{aligned}\tag{4.56}$$

$$\begin{aligned}(\Pi^D_t)^\mu_\mu &= \frac{g^2_{VNN}}{4\pi^2}\left(\frac{\kappa_V}{2M}\right)^2\frac{k^2}{|\vec{k}|}\int\frac{pdp}{\omega_p}\,\Bigg[(k^2+8M^{*2})\\ &\quad\times\ln\left\{\frac{(k^2+2|\vec{p}||\vec{k}|)^2-4k_0^2\omega_p^2}{(k^2-2|\vec{p}||\vec{k}|)^2-4k_0^2\omega_p^2}\right\}-4|\vec{p}||\vec{k}|\Bigg]\\ &\quad\times\Big[\,f_{BE}(\mu^*,T)+\bar{f}_{BE}(\mu^*,T)\Big]\end{aligned}\tag{4.57}$$

The longitudinal component of the polarization tensor is given by

$$\Pi^D_L=\Pi^{D,v}_L+\Pi^{D,vt}_L+\Pi^{D,t}_L\tag{4.58}$$

with

$$\begin{aligned}\Pi^{D,v}_L &= -\frac{g^2_{VNN}}{4\pi^2}\frac{k^2}{|\vec{k}|^3}\int\frac{pdp}{\omega_p}\,\Bigg[\{(k_0-2\omega_p)^2-|\vec{k}|^2\}\ln\frac{k^2-2k_0\omega_p+2|\vec{p}||\vec{k}|}{k^2-2k_0\omega_p-2|\vec{p}||\vec{k}|}\\ &\quad+\{(k_0+2\omega_p)^2-|\vec{k}|^2\}\ln\frac{k^2+2k_0\omega_p+2|\vec{p}||\vec{k}|}{k^2+2k_0\omega_p-2|\vec{p}||\vec{k}|}-8|\vec{p}||\vec{k}|\Bigg]\\ &\quad\times\Big[\,f_{BE}(\mu^*,T)+\bar{f}_{BE}(\mu^*,T)\Big]\end{aligned}\tag{4.59}$$

whereas,

$$\begin{aligned}\Pi^{D,vt}_L &= \frac{g^2_{VNN}}{\pi^2}M^*\left(\frac{\kappa_V}{2M}\right)\frac{k^2}{|\vec{k}|}\int\frac{pdp}{\omega_p}\,\ln\left\{\frac{(k^2+2|\vec{p}||\vec{k}|)^2-4k_0^2\omega_p^2}{(k^2-2|\vec{p}||\vec{k}|)^2-4k_0^2\omega_p^2}\right\}\\ &\quad\times\Big[\,f_{BE}(\mu^*,T)+\bar{f}_{BE}(\mu^*,T)\Big]\end{aligned}\tag{4.60}$$

and finally,

$$\begin{aligned}\Pi_L^{D,t} &= -\frac{g_{VNN}^2}{2\pi^2}\left(\frac{\kappa_V}{2M}\right)^2\frac{k^2}{|\vec{k}|}\int\frac{pdp}{\omega_p}\left[\left\{2|\vec{p}|^2-\frac{k^2}{2}-\frac{(k^2-2k_0\omega_p)^2}{2|\vec{k}|^2}\right\}\right.\\ &\times\ln\frac{k^2-2k_0\omega_p+2|\vec{p}||\vec{k}|}{k^2-2k_0\omega_p-2|\vec{p}||\vec{k}|}+\left\{2|\vec{p}|^2-k^2-\frac{(k^2+2k_0\omega_p)^2}{|\vec{k}|^2}\right\}\\ &\left.\times\ln\frac{k^2+2k_0\omega_p+2|\vec{p}||\vec{k}|}{k^2+2k_0\omega_p-2|\vec{p}||\vec{k}|}-\frac{4|\vec{p}|k_0^2}{|\vec{k}|}\right]\\ &\times\Big[f_{BE}(\mu^*,T)+\bar{f}_{BE}(\mu^*,T)\Big] \qquad (4.61)\end{aligned}$$

The dispersion relation for the longitudinal (transverse) mode now reads

$$k_0^2-|\vec{k}|^2-m_V^2+\mathrm{Re}\Pi_{L(T)}^D(k_0,\vec{k})+\mathrm{Re}\Pi^F(k^2)=0 \qquad (4.62)$$

Usually the physical mass (m_V^*) is defined as the lowest zero of the above equation in the limit $\vec{k}\to 0$. In this limit $\Pi_T^D=\Pi_L^D=\Pi^D$, and we have,

$$\frac{1}{3}\Pi_\mu^\mu=\Pi=\Pi^D+\Pi^F \qquad (4.63)$$

where

$$\Pi^D(k_0,\vec{k}\to 0)=-\frac{4g_{VNN}^2}{\pi^2}\int p^2dp\,F(|\vec{p}|,M^*)\,[\,f_{BE}(\mu^*,T)+\bar{f}_{BE}(\mu^*,T)] \qquad (4.64)$$

with

$$\begin{aligned}F(|\vec{p}|,M^*) &= \frac{1}{\omega_p(4\omega_p^2-k_0^2)}\left[\frac{2}{3}(2|\vec{p}|^2+3M^{*2})+k_0^2\left\{2M^*(\frac{\kappa_V}{2M})\right.\right.\\ &+\left.\left.\frac{2}{3}(\frac{\kappa_V}{2M})^2(|\vec{p}|^2+3M^{*2})\right\}\right] \qquad (4.65)\end{aligned}$$

where $\omega_p^2=\vec{p}^2+M^{*2}$.

The effective mass of the vector meson is then obtained by solving the equation:

$$k_0^2-m_V^2+\mathrm{Re}\Pi=0. \qquad (4.66)$$

The effective masses take the following parametrised forms:

$$\begin{aligned}m_\rho^* &= m_\rho\left[1-0.127\left(\frac{T(\mathrm{GeV})}{0.16}\right)^{5.24}\right]\\ m_\omega^* &= m_\omega\left[1-0.0438\left(\frac{T(\mathrm{GeV})}{0.16}\right)^{7.09}\right]. \qquad (4.67)\end{aligned}$$

One finds reference to two other kinds of masses in the literature. The invariant mass is defined as the lowest order zero of Eq. 4.62 with Π^D neglected. Again, the screening mass of a vector meson is obtained from the pure imaginary zero of the quantity on the left hand side of the same equation with $k_0=0$. These two masses are different because of the non-analyticity of the polarization tensor at the origin *i.e.* at $(p_0,\vec{p})=(0,\vec{0})$.

5 Spectral Constraints at Finite T

In the previous section we have discussed the change in hadronic properties using effective Lagrangian approach (QHD). However, medium modifications can also be studied by applying QCD sum rules (QSR) [90, 91, 92]. As many good reviews are available on the QSR at zero temperature [33, 93, 94, 95, 96] after the original work of Shifman et al [97], we, therefore, introduce only the basic principles of QSR in the thermal bath.

5.1 QCD Sum Rule at Non-zero Temperature

QCD sum rules for vector mesons in medium [91, 92] start with the retarded current correlation function,

$$\Pi^R_{\mu\nu}(q_0,\vec{q}) = i\int d^4x e^{iqx}\theta(x_0)\langle\,[J_\mu(x),J_\nu(0)]\,\rangle\ , \tag{5.1}$$

where $q^\mu \equiv (q_0,\vec{q})$ is the four momentum, with the source (electromagnetic) currents J_μ defined in terms of the quark fields as (in units of e),

$$J_\mu = \frac{2}{3}\bar{u}\gamma_\mu u - \frac{1}{3}\bar{d}\gamma_\mu d - \frac{1}{3}\bar{s}\gamma_\mu s \tag{5.2}$$

Defining the current in the ρ, ω and ϕ channels as

$$J^\rho_\mu = (1/2)(\bar{u}\gamma_\mu u - \bar{d}\gamma_\mu d), \tag{5.3}$$

$$J^\omega_\mu = (1/2)(\bar{u}\gamma_\mu u + \bar{d}\gamma_\mu d), \tag{5.4}$$

and

$$J^\phi_\mu = \bar{s}\gamma_\mu s, \tag{5.5}$$

one can express the electromagnetic current in terms of ρ, ω and ϕ fields as,

$$J_\mu = J^\rho_\mu + \frac{1}{3}J^\omega_\mu - \frac{1}{3}J^\phi_\mu, \tag{5.6}$$

As discussed earlier there are two independent invariants in medium, the transverse (Π^R_T) and the longitudinal (Π^R_L) components of the polarization tensor. In the limit $\vec{q}\to 0$, as there is no spatial direction, Π^R_T and Π^R_L becomes equal ($=\Pi^R$) and the trace of the retarded correlation function can be expressed in terms of Π^R as $\Pi^R \equiv \Pi^{\mu R}_\mu/(-3q_0^2)$. Both the transverse and the longitudinal components satisfy the fixed $\vec{q}$ dispersion relation. In particular, at $\vec{q}=0$,

$$\mathrm{Re}\Pi^R(q_0) = \frac{1}{\pi}\mathrm{P}\int_0^\infty du^2 \frac{\mathrm{Im}\Pi^R(u)}{u^2-q_0^2} + (\text{subtraction}). \tag{5.7}$$

$\mathrm{Re}\Pi^R$ can be calculated using perturbation theory with power corrections (operator product expansion (OPE)) in the deep Euclidian region $q_0^2\to-\infty$. For example,

OPE for $\mathrm{Re}\Pi^R(q_0)$, which is the same with the OPE for the causal (Feynman) correlator $\Pi^F(q_0)$, has a general form at $q_0^2 \equiv -Q^2 \to -\infty$,

$$\mathrm{Re}\Pi^R(q_0^2 \to -\infty) = -C_0 \ln Q^2 + \sum_{n=1}^{\infty} \frac{C_n(\alpha_s(\mu^2), \ln(\mu^2/Q^2))}{Q^{2n}} \langle \mathcal{O}_n(\mu^2) \rangle_T \quad , \quad (5.8)$$

where μ is the renormalization point of the local operators, which separates the hard scale $|\omega|$ and soft scales such as Λ_{QCD} and T. C_n are the c-number Wilson coefficients which are T independent. All the medium effects are contained in the thermal average of the local operators $\mathcal{O}_n$. Since $\langle \mathcal{O}_n \rangle_T \sim T^{2l} \cdot \Lambda_{QCD}^{2m}$ with $l+m=n$ due to dimensional reasons, (5.8) is a valid asymptotic expansion as far as $Q^2 \gg T^2$ and Λ_{QCD}^2. The local operators $\mathcal{O}_n(\mu^2)$ in the vector meson sum rule are essentially the same with those in the lepton-nucleon deep inelastic scattering (DIS) and can be characterized by their canonical dimension (d) and the twist (τ=dimension-spin). They are given in [92] up to dimension 6 operators and we will not recapitulate them here. For $\vec{q} \to 0$, Eq. 5.8 is an asymptotic series in $1/\omega^2$ or equivalently an expansion with respect to d. The medium condensates $\langle \mathcal{O}_n(\mu^2) \rangle_T$ may be evaluated by low energy theorems, the parton distribution of hadrons and lattice QCD simulations.

Matching the l.h.s. and the r.h.s. of eq. (5.7) in the asymptotic region $\omega^2 \to -\infty$ is the essential part of QSR. This procedure gives constraints on the spectral integral and hence the hadronic properties in the medium as well as in the vacuum. There are two major procedures for this matching, namely the Borel sum rules (BSR) [97] and the finite energy sum rules (FESR) [98], which can be summarized as

$$\int_0^{\infty} dq_0^2 \;\; W(q_0^2) \quad [\mathrm{Im}\Pi^R(q_0) - \mathrm{Im}\Pi^R_{OPE}(q_0)] = 0, \quad (5.9)$$

$$W(s) \quad = \begin{cases} q_0^{2n}\, \theta(S_0 - q_0^2) & \text{(FESR)}, \\ e^{-q_0^2/M^2} & \text{(BSR)}. \end{cases}$$

Here $\mathrm{Im}\Pi^R_{OPE}(q_0)$ is a hypothetical imaginary part of Π^R obtained from OPE.

In QSR in the vacuum, the spectral function (i.e. $\mathrm{Im}\Pi^R$ in Eq.5.7) is usually modeled with a resonance pole and the continuum to extract the mass and decay constant of hadrons. In the medium, such a simple parametrization is not always justified because of the thermal broadening of the spectrum and also because of the new spectral structure due to Landau damping and the thermal mixing among mesons. Therefore, the model independent constraints obtained from QSR are only for the weighted spectral integral.

For example, the first three finite energy sum rules at finite T read [92]

$$I_1 = \int_0^{\infty} [\mathrm{Im}\Pi^R(q_0) - \mathrm{Im}\Pi^R_{OPE}(q_0)]\; dq_0^2 = 0, \quad (5.10)$$

$$I_2 = \int_0^{\infty} [\mathrm{Im}\Pi^R(q_0) - \mathrm{Im}\Pi^R_{OPE}(q_0)]\; q_0^2\; dq_0^2 = -C_2 \langle \mathcal{O}_2 \rangle_T, \quad (5.11)$$

$$I_3 = \int_0^{\infty} [\mathrm{Im}\Pi^R(q_0) - \mathrm{Im}\Pi^R_{OPE}(q_0)]\; q_0^4\; dq_0^2 = C_3 \langle \mathcal{O}_3 \rangle_T. \quad (5.12)$$

Similar sum rules hold for the axial vector channel (in the chiral limit) except that one has a different operator for $\mathcal{O}_3$. One can also generalize the above sum rules to finite $\vec{q}$ [99, 100].

Explicit forms of $C_n\langle\mathcal{O}_n\rangle_T$ have been calculated as [92]

$$C_0 = -\frac{1}{8\pi}(1+\frac{\alpha_s}{\pi}), \quad C_1 = 0, \tag{5.13}$$

$$C_2\langle\mathcal{O}_2\rangle_T = \frac{1}{24}\langle\frac{\alpha_s}{\pi}G^2\rangle_T + \frac{4}{3}\langle\mathcal{S}\bar{q}i\gamma_0 D_0 q\rangle_T, \tag{5.14}$$

$$C_3\langle\mathcal{O}_3\rangle_T = -\langle\text{scalar } 4-\text{quark})\rangle_T + \frac{16}{3}\langle\mathcal{S}\bar{q}i\gamma_0 D_0 D_0 D_0 q\rangle_T. \tag{5.15}$$

Here we have neglected the terms proportional to the light quark masses and the quark-gluon mixed operators. Also, $\mathcal{S}$ makes the operators symmetric and traceless. At low T, one may use the soft pion theorems and the parton distribution of the pion to estimate the r.h.s. of the above equations. When T is close to T_c, one has to look for a totally different way of estimation: the simplest approach is to assume the resonance gas to evaluate the r.h.s., while the direct lattice simulations will be the most reliable way in the future. An important feature of the OPE in the above is the appearance of local operators with Lorentz indices. This happens because we are taking the rest frame of the heat bath which breaks covariance.

The sum rules I_i can be used to check the validity of the calculations of the spectral functions using effective theories of QCD. This is in fact quite useful for the spectral function at finite baryon density. At finite T, especially near the critical point, the behavior of the condensates with dim. ≥ 4 is not known precisely. Therefore, it is rather difficult to make a strong argument on the spectral constraints near T_c at present. The future lattice simulations of these condensates are highly called for.

5.2 Parametrization of the Spectral Functions

As mentioned in the introduction the photon and dilepton emission is determined by the retarded correlator of electromagnetic current. In this section we will introduce a parametrization of the correlator at finite T. The parametrization should be consistent with the experimental data from $e^+e^- \to hadrons$ processes at zero T, and it should be also consistent with the high energy behaviour known from perturbative QCD at $\omega \gg T$.

As the vector mesons appear as resonances in the electromagnetic correlator, using Eqs. 5.1 and 5.6 we can write,

$$\text{Im}\Pi^R_{\mu\nu} = \text{Im}\Pi^{R,\rho}_{\mu\nu} + \frac{1}{9}\text{Im}\Pi^{R,\omega}_{\mu\nu} + \frac{1}{9}\text{Im}\Pi^{R,\phi}_{\mu\nu}. \tag{5.16}$$

The above equation shows that the contributions of ω and ϕ mesons to the electromagnetic probes are down by almost an order of magnitude compared to ρ mesons.

As mentioned before, at zero three momentum the imaginary part of the trace of the retarded correlator can be written in terms of its longitudinal component as,

$$\text{Im } \Pi^R_{\mu\mu}(q_0) = -3q_0^2 \text{ Im } \Pi^R_L(q_0). \tag{5.17}$$

Thus our next task is to parametrize $\text{Im}\Pi^R_L(\omega)$. We take a Breit-Wigner form with an energy-dependent width for the resonance along with a continuum:

$$\text{Im } \Pi^\rho_L(q_0, \vec{q}=0) = f_\rho^2 \frac{D_\rho}{(q_0^2 - m_\rho^2)^2 + D_\rho^2} + \frac{1}{8\pi}(1 + \frac{\alpha_s}{\pi}) \frac{1}{1 + e^{(\omega_0 - q_0)/\delta}}. \tag{5.18}$$

At zero T, this reduces to a relativistic generalization of the parameterization used by Shuryak [32] to fit the experimental data of $e^+e^- \to hadrons$. Here D_ρ is the imaginary part of the self-energy which should in principle contain all the channels which can destroy or create a ρ in the thermal bath. Hence D_ρ is given by the difference of the decay-width and the formation width and is given by $D_\rho = q_0\Gamma(q_0)$. However, we have seen that for a baryon free matter the most dominant contribution to D_ρ comes from the pion-loop [101]. For a rho meson propagating with energy ω and three momentum $\vec{q}$ the rho width is given by

$$\begin{aligned} \Gamma_{\rho\to\pi\pi}(q_0, \vec{q}) &= \frac{g^2_{\rho\pi\pi}}{48\pi} W^3(s) \frac{s}{q_0} \left[1 + \frac{2T}{W(s)\sqrt{q_0^2 - s}} \right. \\ &\left. \times \ln \left\{ \frac{1 - \exp[-\frac{\beta}{2}(q_0 + W(s)\sqrt{q_0^2 - s})]}{1 - \exp[-\frac{\beta}{2}(q_0 - W(s)\sqrt{q_0^2 - s})]} \right\} \right] \end{aligned} \tag{5.19}$$

where $s = q_0^2 - \vec{q}^2$ and $W(s) = \sqrt{1 - 4m_\pi^2/s}$. In the limit $|\vec{q}| \to 0$, the above expression reduces to the in-medium decay width and is given by

$$\Gamma_{\rho\to\pi\pi}(q_0) = \frac{g^2_{\rho\pi\pi}}{48\pi} q_0 W^3(q_0) \left[\left(1 + f_{BE}(\frac{q_0}{2}) \right) \left(1 + f_{BE}(\frac{q_0}{2}) \right) - f_{BE}(\frac{q_0}{2}) f_{BE}(\frac{q_0}{2}) \right] \tag{5.20}$$

with $f_{BE}(x) = [e^x - 1]^{-1}$, ω_0 is the continuum threshold above which the asymptotic freedom is restored and f_ρ is the coupling between electromagnetic current and the ρ field defined as

$$\langle 0 \mid J^\rho_\mu \mid \rho \rangle = f_\rho m_\rho \epsilon_\mu \tag{5.21}$$

Assuming vector dominance in the medium we obtain,

$$g_\rho = m_\rho / f_\rho \tag{5.22}$$

In the vacuum, the standard parameters for the ρ spectral function are given by, $m_\rho = 0.77$ GeV, $m_\pi = 0.14$ GeV , $f_\rho = 0.141$ GeV, $g_\rho = 5.46$, $\omega_0 = 1.3$ GeV, $\delta = 0.2$ GeV and $\alpha_s = 0.3$. Resulting spectral function for the ρ-meson *in the vacuum* should be compared with Ref. [33].

Let us now concentrate on the spectral function in the omega channel. We again take a Breit-Wigner form along with a continuum:

$$\text{Im } \Pi_L^{R,\omega}(q_0, \vec{q}=0) = f_\omega^2 \frac{D_\omega(q_0)}{(q_0^2 - m_\omega^2)^2 + D_\omega(q_0)^2} + \frac{1}{8\pi}(1 + \frac{\alpha_s}{\pi}) \frac{1}{1 + e^{(\omega_0 - q_0)/\delta}} \quad (5.23)$$

where f_ω is a coupling of the current with the ω-meson defined as

$$\langle 0 \mid J_\mu^\omega \mid \omega \rangle = f_\omega m_\omega \epsilon_\mu. \quad (5.24)$$

Note that f_ω here is defined as factor 3 larger than Shuryak's definition [32] . D_ω, which is the imaginary part of the self-energy, is calculated using the Lagrangian density given in Eq. 3.10. We have shown in earlier calculations [101, 102] that a substantial contribution to the omega width comes from the process $\omega\pi \to \pi\pi$ in a thermal bath. Consequently

$$D_\omega(q_0) = q_0(\Gamma_{\omega \to 3\pi} + \Gamma_{\omega\pi \to \pi\pi}) \quad (5.25)$$

where

$$\Gamma_{\omega \to 3\pi}(q_0) = C \int_{w_{min}}^{w_{max}} dw \int_{x_{min}}^{x_{max}} dx \mid F \mid^2 S \quad (5.26)$$

S is the phase space factor for thermal equilibrium, given by

$$S = [(1 + f_{BE}(E_1))(1 + f_{BE}(E_2))(1 + f_{BE}(E_3)) - f_{BE}(E_1) f_{BE}(E_2) f_{BE}(E_3)] \quad (5.27)$$

and

$$C = \frac{g_{\omega\rho\pi}^2 \, g_{\rho\pi\pi}^2 \, q_0}{48\pi^3 \, m_\pi^2} \quad (5.28)$$

The limits of integration are

$$\begin{aligned}
w_{\min} &= m_\pi, \\
w_{\max} &= (q_0^2 - 3m_\pi^2)/2\, q_0, \\
x_{\max} &= \sqrt{0.5\omega\,(w - w_{\max})(w^2 - m_\pi^2)/(2q_0\, w - q_0^2 - m_\pi^2)}, \\
x_{\min} &= -x_{\max}, \\
E_1 &= w, \\
E_2 &= x + (q_0 - w)/2, \\
E_3 &= -x + (q_0 - w)/2, \\
\mid \vec{p}_i \mid &= \sqrt{E_i^2 - m_\pi^2},
\end{aligned} \quad (5.29)$$

and $\vec{p}_i$ is the pion 3-momentum. The amplitude for the process is

$$\mid F \mid^2 = \mid \vec{p}_1 \mid^2 \mid \vec{p}_2 \mid^2 (1 - Z_0^2) H \quad (5.30)$$

where

$$Z_0 = \frac{\omega^2 + m_\pi^2 - 2\omega(E_1 + E_2) + 2E_1E_2}{2 \mid \vec{p}_1 \vec{p}_2 \mid} \quad (5.31)$$

and

$$H = \sum_{i=1}^{6} h_i \tag{5.32}$$

with

$$\begin{aligned}
h_1 &= \frac{1}{q_{12}^2 + m_\rho^2 \Gamma_\rho^2} \\
h_2 &= \frac{1}{q_{13}^2 + m_\rho^2 \Gamma_\rho^2} \\
h_3 &= \frac{1}{q_{23}^2 + m_\rho^2 \Gamma_\rho^2} \\
h_4 &= 2(q_{12}q_{13} + m_\rho^2\Gamma_\rho^2)h_1h_2 \\
h_5 &= 2(q_{13}q_{23} + m_\rho^2\Gamma_\rho^2)h_2h_3 \\
h_6 &= 2(q_{12}q_{23} + m_\rho^2\Gamma_\rho^2)h_1h_3 \\
q_{12} &= (E_1 + E_2)^2 - \vec{p}_3^{\,2} - m_\rho^2 \\
q_{13} &= (E_1 + E_3)^2 - \vec{p}_2^{\,2} - m_\rho^2 \\
q_{23} &= (E_2 + E_3)^2 - \vec{p}_1^{\,2} - m_\rho^2
\end{aligned} \tag{5.33}$$

The width for $\omega\pi \to \pi\pi$ is calculated analogously.

In the vacuum the standard parameters for ω are as follows. $m_\omega = 0.782$ GeV, $m_\pi = 0.14$ GeV, $f_\omega = 0.138$ GeV, $\omega_0 = 1.1$ GeV, $\delta = 0.2$ GeV and $\alpha_s = 0.3$.

In a medium at finite T, we simply replace m_ρ, ω_0,f_ρ and g_ρ by the corresponding effective quantities (denoted by asterix) m_ρ^*, ω_0^*, f_ρ^* and g_ρ^*. Since not much is known about the critical behavior of the scalar and tensor condensates at finite T in QCD sum rules we take a simple ansatz for in-medium quantities for their T-dependence. A possible parametrization of $*$-quantities at finite T is

$$\frac{m_V^*}{m_V} = \frac{f_V^*}{f_V} = \frac{\omega_0^*}{\omega_0} = \left(1 - \frac{T^2}{T_c^2}\right)^\lambda, \tag{5.34}$$

where λ is a sort of *dynamical* critical exponent and V stands for vector mesons (ρ and ω). (Note that there is no definite reason to believe that all the in-medium dynamical quantities are dictated by a single exponent λ. This is a simplest possible ansatz.) Since the numerical value of λ is not known, we take two typical cases: $\lambda = 1/6$ (BR scaling) and $1/2$ (Nambu scaling) [34].

Some remarks are in order here:
(i) Eq.(5.34) for m_ρ^* is not entirely consistent with the low temperature theorem [103], which says there should be no $O(T^2)$ correction to the mass. Therefore, one cannot take the ansatz too seriously at low T. In practical applications, however, $T < 100$ MeV is not relevant in any way since it is below the freeze-out temperature.
(ii) Local duality constraint I_1 in QCD sum rules implies that $(f_\rho^*)^2 = 8\pi^2(1 + \alpha_s/\pi)(\omega_0^*)^2 + (\text{scattering term})$ [92]. This condition is slightly violated for f_ρ^* in Eq. 5.34 because of the existence of the scattering term (Landau damping).

(iii) The vector dominance assumption in the medium together with Eq. 5.34 simply leads to $g_\rho^* = g_\rho$.

Under these reservations, we will use the parametrized spectral functions (BR scaling and Nambu scaling) in the calculation of the lepton and photon productions in later sections. Major qualitative difference between the spectral function in QHD and that in this section is the existence of the continuum and its medium modification at finite T.

Dilepton emission involving the rho and omega mesons is obtained by inserting e^2 times Eqs. 5.18 and 5.23 in Eq. 3.12 using Eq. 5.17.

6 Evolution Dynamics

As mentioned earlier, in URHICs the produced matter will either be in the form of a hot hadronic gas or a quark gluon plasma. So far we have talked about the rate of photon and dilepton emission per unit time from unit volume of a thermal system made up of quark matter and hadronic matter at a fixed temperature T. Our next task is to consider its evolution in space and time. This is done using relativistic hydrodynamics. A basic ingredient of the hydrodynamic description of the collision volume is the existence of a strong interaction time scale,

$$\tau_i \sim \frac{1}{\Lambda_{QCD}} \sim 1\text{fm/c} \sim \tau_{\text{formation}} \tag{6.1}$$

In any hadronic collision the produced fragments can only interact after a proper time τ_i has elapsed after their collisions. Thus, there is another time scale in the problem, the so called transit time , which is defined as

$$\tau_{\text{transit}} \sim \frac{2R_A}{\gamma_{\text{cm}}} \tag{6.2}$$

R_A is the nuclear radius, γ_{cm} is the Lorentz factor. If the value of γ_{cm} (which is a function of the collision energy) is such that $\tau_{\text{transit}} < \tau_{\text{formation}}$ then most of the secondaries are formed after the nuclei pass through each other. Consequently these secondaries will not contribute to the energy density of the fluid in the central region. Such a scenario may be realised in RHIC and LHC energies. This particular feature has been taken into account in Bjorken's hydrodynamic model.

6.1 Bjorken's Hydrodynamical Model

It has been observed experimentally that the particle spectra for the secondaries produced in $N-N$ collisions exhibit a central plateau in the rapidity space. This kind of behaviour is due to the frame independence symmetry of the hydrodynamic expansion of the system [104]. Bjorken assumed that the same kind of plateau will also be observed in nucleus nucleus collisions [105]. In terms of the initial condition this means that the energy density, pressure etc (all the thermodynamic quantities)

will be a function of the initial thermalization (proper) time τ_i only and *will not* depend on the space time rapidity η (defined later). This initial symmetry of the thermodynamic quantities is preserved throughout the evolution scenario. If the particle rapidity density is flat or invariant under Lorentz boosts then the entropy density (s) will be independent of the rapidity. Since our discussion is limited to the baryon free region, there is only one independent thermodynamic variable T, say. Once s is independent of Lorentz boost (rapidity) so are all the thermodynamic quantities.

The evolution of the fluid is governed by the energy momentum conservation equation

$$\partial_\mu T^{\mu\nu} = 0 \tag{6.3}$$

where $T^{\mu\nu} = (\epsilon + P)u^\mu u^\nu + g^{\mu\nu}P$ is the energy momentum tensor for ideal fluid. For an isentropic flow the entropy conservation reads

$$\partial_\mu s^\mu = 0 \tag{6.4}$$

where $s^\mu = s\,u^\mu$ is the entropy current. Let us consider the frame independence symmetry in a two dimensional sub-space ($t - z$ plane). Changing the independent variables from (t, z) to (τ, η) using

$$\tau = \sqrt{t^2 - z^2}; \quad \eta = \frac{1}{2}\ln\frac{t+z}{t-z} \tag{6.5}$$

the equation of motion Eqs. 6.3 and 6.4 become

$$\frac{\partial}{\partial\tau}\left(s\tau\cosh(y-\eta)\right) + \frac{\partial}{\partial\eta}\left(s\sinh(y-\eta)\right) = 0 \tag{6.6}$$

$$\frac{\partial}{\partial\tau}\left(T\tau\sinh(y-\eta)\right) + \frac{\partial}{\partial\eta}\left(T\cosh(y-\eta)\right) = 0 \tag{6.7}$$

The independent variable τ, by definition is the proper time of the frame which is related to the c.m. frame by a Lorentz transformation along the z-axis with velocity z/t. The variable η, known as the space time rapidity, becomes equal to the fluid rapidity $y(= \frac{1}{2}\ln(1+v_z)/(1-v_z))$. Putting $y = \eta$ in Eqs. 6.6 and 6.7 we get

$$\frac{\partial}{\partial\tau}\left(s\tau\right) = 0 \tag{6.8}$$

$$\frac{\partial T}{\partial\eta} = 0 \tag{6.9}$$

These equations imply that T is independent of η and so are all the thermodynamic quantities and $s\tau$ =const. This is the Bjorken's scaling solution. The resulting space-time picture of the collision is shown in Fig. (5).

It may be noted that the above results were obtained without any specific input from the equation of state (EOS), it is thus a general result that one dimensional similarity flow is necessarily isentropic even if there is a phase transition. For a

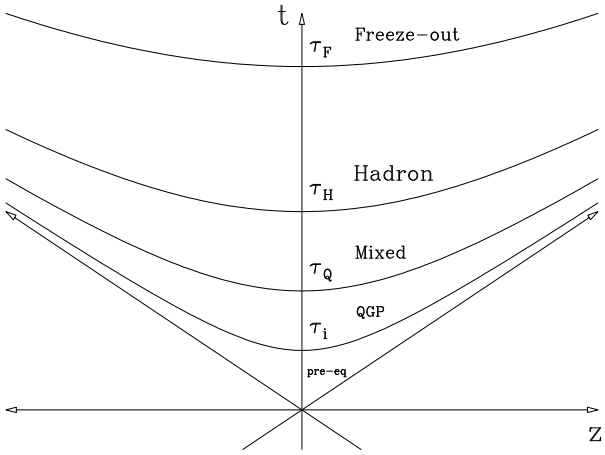

Figure 5: Space-time diagram of the collision in Bjorken hydrodynamics

relativistic massless gas with statistical degeneracy g, s and T are related through the equation of state:

$$s = 4\frac{\pi^2}{90} g T^3 \tag{6.10}$$

Putting this expression for entropy density in the Bjorken scaling solution we get $T^3\tau$ =const. This is the cooling law which is routinely used to evaluate the signals of QGP. The initial temperature of the system is determined by observing that the variation of temperature from its initial value T_i to final value T_f (freeze-out temperature) with proper time (τ) is governed by the entropy conservation (Eq. 6.8)

$$s(T)\tau = s(T_i)\tau_i \tag{6.11}$$

The entropy density is then expressed in terms of the observed particle (pion) multiplicity. Using Eqs. 6.10 and 6.11 one gets the initial temperature as

$$T_i^3 = \frac{2\pi^4}{45\zeta(3)\pi\, R_A^2 4 a_k \tau_i} \frac{dN_\pi}{dy} \tag{6.12}$$

where dN_π/dy is the total pion multiplicity, R_A is the radius of the system, τ_i is the initial thermalization time, and $\zeta(3)$ is the Reimann zeta function. $a_k = (\pi^2/90)\, g_k$ is the degeneracy of the produced system and hence k stands for either QGP or a hot hadronic gas. The rapidity density for the secondaries is obtained from[106],

$$\left(\frac{dN}{dy}\right)_{A-A} = A^\alpha \left(\frac{dN}{dy}\right)_{p-p} \tag{6.13}$$

where α is known as the rescattering parameter. $dN/dy\,|_{p-p}$ can be parameterized to fit the experimental data in the central region as

$$\left(\frac{dN}{dy}\right)_{p-p} = 0.8 \ln(\sqrt{s}) \tag{6.14}$$

The assumption of a central plateau in the rapidity distribution is not experimentally observed in nucleus nucleus collisions at the presently available energies. Hence the boost invariant hydrodynamics may not be a valid concept at these energies. The concept of complete stopping in Landau model [107] is not valid either at these energies. The physical situation may be in between the boost invariant model of Bjorken and the Landau model of complete stopping, which means that there may be an overlap between the formation zone and the collision zone. For its simplicities the Bjorken model will be used in this work to describe the space time evolution of matter formed in URHICs. Appropriate generalization has been made to take into account the temperature dependent hadronic masses.

6.2 Initial Conditions and Equation of State

The set of hydrodynamic equations is not closed by itself; the number of unknown variables exceeds the number of equations by one. One thus needs to postulate a functional relation between any two variables so that the system becomes deterministic. The most natural course is to look for such a relation between the pressure P and the energy density ϵ, as is done in the case of thermal equilibrium. Under the assumption of local thermal equilibrium, this functional relation between P and ϵ is the EOS. Obviously, different EOS's will govern the hydrodynamic flow quite differently [108] and as far as the search for QGP is concerned, the goal is to look for distinctions in the observables due to the different EOS's (corresponding to the novel state of QGP vis-a-vis that for the usual hadronic matter). It is thus imperative to understand in what respects the two EOS's differ and how they affect the evolution in space and time. Recently, the sensitivity of the photon emission rate on various evolution scenarios has been studied in Ref. [109].

A physically intuitive way of understanding the role of the EOS in governing the hydrodynamic flow lies in the fact that the velocity of sound $c_s^2 = (\partial P/\partial\epsilon)_s$ sets an intrinsic scale in the hydrodynamic evolution. One can thus write a simple parametric form for the EOS: $P = c_s^2(T)\epsilon$. Inclusion of interactions, however, may drastically alter the value of c_s^2 [110]. In our calculation we assume the MIT bag model equation of state for the QGP where the energy density and pressure are given by

$$\epsilon_Q = g_Q \frac{\pi^2 T^4}{30} + B, \tag{6.15}$$

and

$$P_Q = g_Q \frac{\pi^2}{90} T^4 - B. \tag{6.16}$$

The effective degrees of freedom in QGP, $g_Q = 37$ for two flavours. The entropy density s_Q is given by $s_Q = 2g_Q(\pi^2/45)T^3$. Putting $a_k \equiv a_Q = (\pi^2/90)g_Q$ the initial temperature for a system produced as QGP can be determined from Eq. 6.12.

In the hadronic phase we have to be more careful about the presence of heavier particles and the change in their masses due to finite temperature effects. The ideal limit of treating the hot hadronic matter as a gas of pions originated from

the expectation that in the framework of local thermalization the system would be dominated by the lowest mass hadrons while the higher mass resonances would be Boltzmann suppressed. Indirect justification of this assumption comes from the experimental observation in high energy collisions that most of the secondaries are pions. Nevertheless, the temperature of the system is higher than m_π during a major part of the evolution and at these temperatures the suppression of the higher mass resonances may not be complete. It may therefore be more realistic to include higher mass resonances in the hadronic sector, their relative abundances being governed by the condition of (assumed) thermodynamic equilibrium. We assume that the hadronic phase consists of π, ρ, ω, η mesons and nucleons. The nucleons and heavier mesons may play an important role in the EOS in a scenario where mass of the hadrons decreases with temperature.

The energy density and pressure for such a system of mesons and nucleons are given by

$$\epsilon_H = \sum_{h=\text{mesons}} \frac{g_h}{(2\pi)^3} \int d^3p\, E_h\, f_{BE}(E_h, T) + \frac{g_N}{(2\pi)^3} \int d^3p\, E_N\, f_{FD}(E_N, T) \qquad (6.17)$$

and

$$P_H = \sum_{h=\text{mesons}} \frac{g_h}{(2\pi)^3} \int d^3p \frac{p^2}{3\, E_h} f_{BE}(E_h, T) + \frac{g_N}{(2\pi)^3} \int d^3p \frac{p^2}{3\, E_N} f_{FD}(E_N, T) \qquad (6.18)$$

where the sum is over all the mesons under consideration and N stands for nucleons and $E_h = \sqrt{p^2 + m_h^2}$. The entropy density is then

$$s_H = \frac{\epsilon_H + P_H}{T} \equiv 4a_{\text{eff}}(T)\, T^3 = 4\frac{\pi^2}{90} g_{\text{eff}}(m^*(T), T) T^3 \qquad (6.19)$$

where g_{eff} is the effective statistical degeneracy. Thus, we can visualise the finite mass of the hadrons having an effective degeneracy $g_{\text{eff}}(m^*(T), T)$. Because of the temperature dependence of the effective degeneracy Eq. 6.12 has to be solved self consistently in order to calculate the initial temperature of the system initially produced as a hot hadronic gas. We thus solve the equation

$$\frac{dN_\pi}{dy} = \frac{45\zeta(3)}{2\pi^4} \pi\, R_A^2 4a_{\text{eff}}(T_i) T_i^3 \tau_i \qquad (6.20)$$

where $a_{\text{eff}}(T_i) = (\pi^2/90)\, g_{\text{eff}}(m^*(T_i), T_i)$. The change in the expansion dynamics as well as the value of the initial temperature due to medium effects enters the calculation of the photon emission rate through the effective statistical degeneracy.

If the energy/entropy density in the fireball immediately after the so-called "formation time" τ_i is sufficiently high, then the matter exists in the form of a QGP. As the hydrodynamic expansion starts, the system begins to cool until the critical temperature T_c is reached at a time τ_Q. At this instant, the phase transition to the hadronic matter starts. Assuming that the phase transition is a first order one, the

released latent heat maintains the temperature of the system at the critical temperature T_c, even though the system continues to expand; the cooling due to expansion is compensated by the latent heat liberated during the process. Together with the possible explosive events, we are neglecting the scenarios of supercooling or superheating. This process continues until all the matter has converted to the hadronic phase at a time τ_H, still at $T = T_c$; from then on, the system continues to expand, governed by the EOS of the hot hadronic matter till the freeze-out temperature T_f at the proper time τ_f. Thus the appearance of the so called mixed phase at $T = T_c$, when QGP and hadronic matter co-exist, is a direct consequence of the first order phase transition. Apart from the role in QGP diagnostics, the possibility of the mixed phase affects also the bulk features of the evolution process.

In the mixed phase, the relative proportion of QGP and hadronic matter must be a function of time; initially the system consists entirely of QGP and at the end, entirely of hot hadronic matter. If we denote the fraction of the QGP by $f_Q(\tau)$, then the entropy in the mixed phase ($s_{\rm mix}$) can be expressed as,

$$s_{\rm mix} = f_Q(\tau) s_Q^c + (1 - f_H(\tau)) s_H^c \tag{6.21}$$

such that at $\tau = \tau_Q$, $f_Q = 1$ and at $\tau = \tau_H$, $f_H = 1 - f_Q = 1$ and the life time of the mixed phase $\tau_{\rm life}^{\rm mixed}$ is $\tau_H - \tau_Q$. Here s_Q^c (s_H^c) denotes the entropy density of QGP (hadronic) phase at T_c. Since scaling law governing the variation of $s(\tau)$ must continue to hold also in the mixed phase, substituting Eq.6.21 in Eq.6.8 we obtain for $T_i > T_c$,

$$f_Q(\tau) = \frac{1}{r-1}\left(r\frac{\tau_Q}{\tau} - 1\right) = \frac{1}{r-1}\left(\frac{\tau_H}{\tau} - 1\right) \tag{6.22}$$

where r ($= g_Q/g_{\rm eff}$) is the ratio of the degeneracy of QGP phase and the effective degeneracy in the hadronic phase. In the above equation we have used the relation $\tau_H = r\tau_Q$, valid for $(1+1)$ dimensional isentropic expansion.

The quantities f_Q and f_H and also be expressed as $f_Q(\tau) = (s - s_H^c)/(s_Q^c - s_H^c)$ is the volume fraction of the QGP sector in the mixed phase and similarly $f_H = (s_Q^c - s)/(s_Q^c - s_H^c)$ is the volume fraction of the hadronic sector in the mixed phase. These quantities ($f_Q(\tau)$ and $f_H(\tau)$), will be required to evaluate the electromagnetic probes from a evolution scenario, QGP$\rightarrow$ mixed phase$\rightarrow$ hadronic phase $\rightarrow$ freeze-out, in the next section.

If $T_i = T_c$, i.e. if the system is formed in the mixed phase with a fraction f_0 of the QGP phase then

$$f_Q(\tau) = \frac{1}{r-1}\left[(1 + (r-1)f_0)\frac{\tau_i}{\tau} - 1\right] \tag{6.23}$$

The mixed phase ends at a proper time $\tau_H^m = (1 + (r-1)f_0)\tau_i$. In case of $s_i < s_H^c$, the value of $f_H(\tau)$ is always unity.

To make our discussion more specific, consider Pb + Pb collisions at CERN SPS energies. If we assume that the matter is formed in the QGP phase with two flavours (u and d), then $g_k = 37$. Taking $dN_\pi/dy = 600$ as measured by the NA49 Collaboration [111] for Pb + Pb collisions, we obtain $T_i = 185$ MeV for $\tau_i = 1$ fm/c.

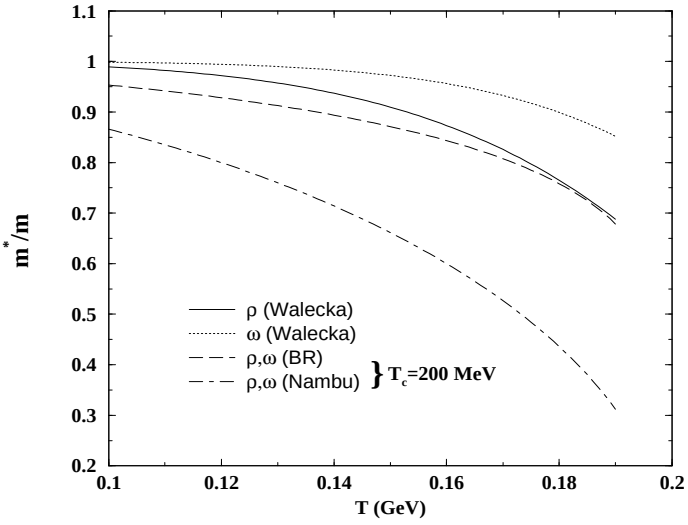

Figure 6: Variation of vector meson mass with temperature for BR (long-dashed line), Nambu (dot-dashed line) scaling with T_c=200 MeV and in the Walecka model for ρ (solid line) and ω (dotted line).

We have taken T_f = 130 MeV [112] in our calculations. We also consider central collisions of Pb + Pb at the RHIC energies which correspond to about 200 GeV/A in the centre of mass system. The particle rapidity density in the central region is taken as 1735 for RHIC. The corresponding initial temperature is (by assuming that $\tau_i = 1$ and QGP initial state) T_i= 265 MeV .

7 Results

7.1 Hadronic properties at non-zero temperature

In the Walecka model the effective nucleon mass at $T \neq 0$ has been evaluated in the Relativistic Hartree Approximation (RHA). Then the ρ and ω masses are computed by evaluating their self energies due to $\rho - N - \bar{N}$ and $\omega - N - \bar{N}$ interaction at finite temperature. The following values of the coupling constants and masses [87] have been used in our calculations: κ_ρ = 6.1, $g^2_{\rho NN}$ = 6.91, m_s= 458 MeV, m_ρ = 770 MeV, M = 939 MeV, g_s^2 = 54.3, κ_ω = 0, and $g_v^2 \equiv g^2_{\omega NN}$ = 102. In Fig. (6) we depict the variation of vector meson masses as a function of temperature in the Walecka model along with the BR and Nambu scaling scenarios. The parametrised forms of the effective masses are given in Eqs. 4.67 and 5.34. The mass variation in the Walecka model and BR scaling is slower than the Nambu scaling scenario. At higher temperature the Walecka model calculation and the BR scaling (near T_c) tend to converge. Such a small difference in the mass variation in the above two scenarios may not be visible through photon spectra. We also note at this point that in the Walecka model ρ and ω mass shows different rate of reduction [70] due to different values of their coupling constants with the nucleons.

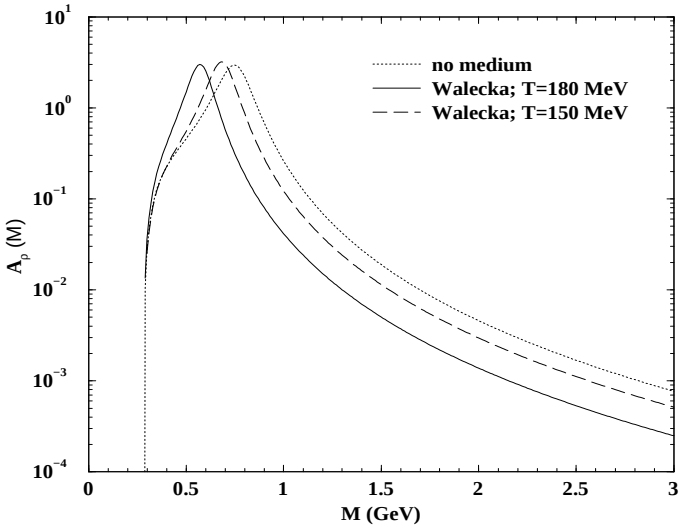

Figure 7: Spectral function of ρ meson in the Walecka model. Solid (long dashed) line corresponds to T =180 MeV (T =150 MeV). The spectral function in vacuum is shown by the dotted line.

In Figs. (7) and (8) the change in the ρ and ω spectral functions at non-zero temperature has been displayed. A_ρ (in units of e) is obtained by multiplying Eq. 3.16 by 8π. A_ω is obtained analogously. We have used the interaction Lagrangians (3.8), (3.10) and (4.18) for this purpose. The shifts in both the spectral functions towards the lower invariant mass region correspond to the reduction of their masses due to thermal interactions (see Fig. 6). The broad ω peak arises due to its interaction with the thermal pion in the heat bath. The reaction $\omega\,\pi \rightarrow \pi\,\pi$ contributes dominantly to the survival probability of the ω in the medium.

Before we proceed further a few comments on Walecka model calculations are in order. In this model the major contribution to the medium effects on the rho and omega mesons arises from the nucleon-loop diagram. For the dressing of internal lines in matter we restrict ourselves to the Mean Field Theory (MFT) to avoid a plethora of diagrams and to maintain internal consistency. It has been shown [47, 52] that the change in the ρ mass due to $\rho - \pi - \pi$ interaction is negligibly small at non-zero temperature and zero baryon density. Therefore the change in the ρ meson mass due to $\rho - \pi - \pi$ interaction is neglected here. At finite baryon density, the dynamics is more involved due to the medium effects on the $\rho - \pi - \pi$ vertex, the pion propagator coupled with delta-hole excitation, and the coupling of the ρ-meson with N^*-hole excitations [113, 114, 115, 116, 117, 118, 119]. (See the review, Ref.[120].) Major effect of such medium modifications is to broaden the ρ-peak as well as to produce complicated structure around the peak. Since in the present work we restrict our calculations within the realm of MFT, *i.e* the internal nucleon loop in the rho and omega self energy is modified due to tadpole diagram only, the inclusion of vertex corrections, modification of the pion propagator and the inclusion of baryon resonaces will take us beyond MFT and hence are not considered here.

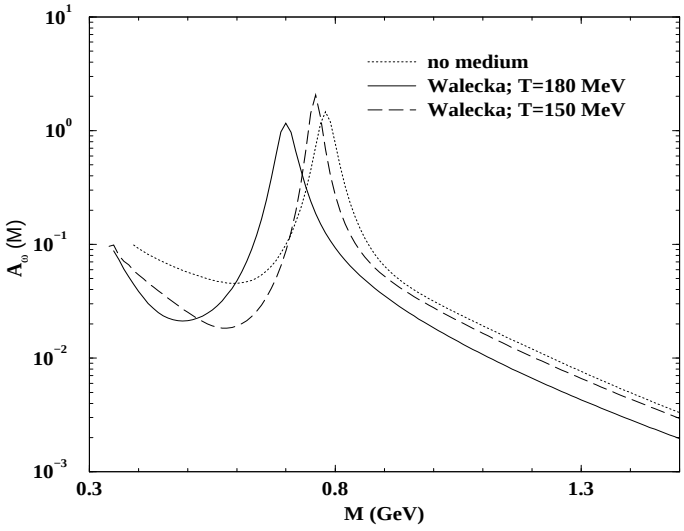

Figure 8: Same as Fig. 7 for the omega.

Also, in the present calculation we restrict to zero baryon density.

In Fig. (9) the spectral function (8π times Eq. 5.18) for the isovector (ρ) channel is plotted as a function of invariant mass at $T = 150$ MeV and $T_c = 160$ MeV. We find that both the peak and the continuum threshold of the spectral function move towards lower invariant mass in case of Nambu scaling as compared to BR scaling. In the case of Nambu scaling the peak of the spectral function and the continuum are not well separated; a merging of the two would take place at $T = T_c$. This could possibly indicate the onset of a deconfinement phase transition. Fig. (10) shows the spectral function at $T = 180$ MeV and $T_c = 200$ MeV. Due to a larger separation between T_c and T compared to the previous case the peaks in the spectral function in all the cases are well separated from the continuum.

In Figs. (11) and (12) the spectral functions for the isoscalar (ω) channel have been depicted. In both the cases the peak in the spectral function is distinctly visible in all the mass variation scenarios. The larger width in the isoscalar channel is due to the combined processes $\omega \to 3\pi$ and $\omega\,\pi \to \pi\,\pi$ as discussed before.

The spectral functions for the vector mesons both in the isoscalar and isovector channels are plotted in Fig. (13) at a temperature $T \sim T_c$. As expected from the scaling law the peak has vanished due to its overlap with the continuum. All the hadrons in the thermal bath have melted to their fundamental constituents - the quarks and gluons. Such a spectral function would indicate a transition from hot hadronic matter to QGP. This behaviour should, in principle, be reflected in the dilepton spectrum originating from these channels. Such broad spectral representation without any peak may be compared with that of huge decay width of the ρ meson due to its interaction with the baryonic medium [121, 122].

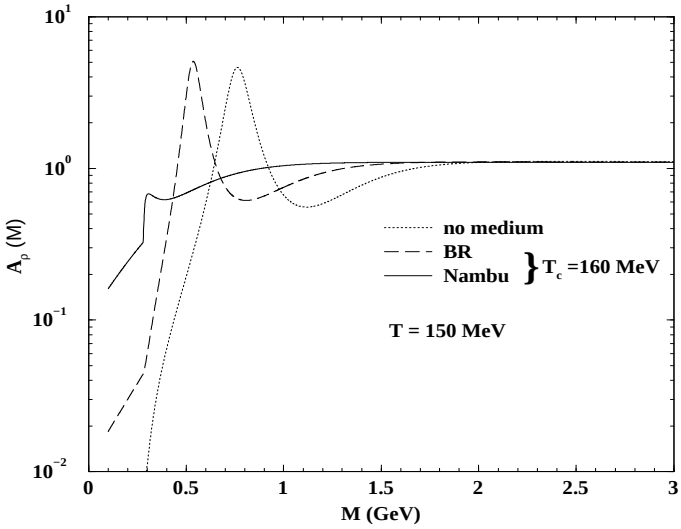

Figure 9: Spectral function for the isovector channel extracted from e^+e^- collisions (dotted line) as a function of invariant mass. The dashed (solid) line indicates the spectral function when m_ρ and ω_0 vary according to BR (Nambu) scaling.

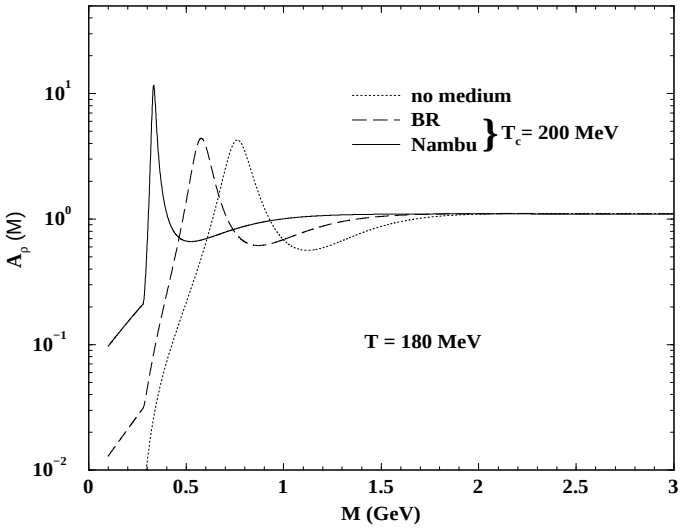

Figure 10: Same as Fig. 9 at $T = 180$ MeV and $T_c = 200$ MeV.

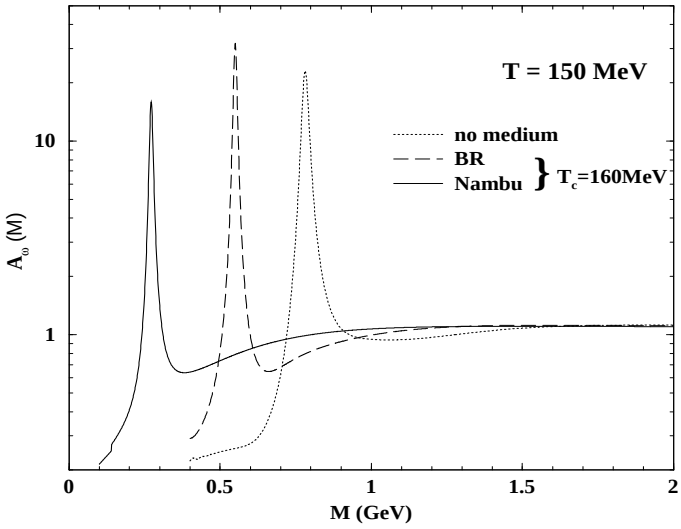

Figure 11: Same as Fig. 9 for the isoscalar channel.

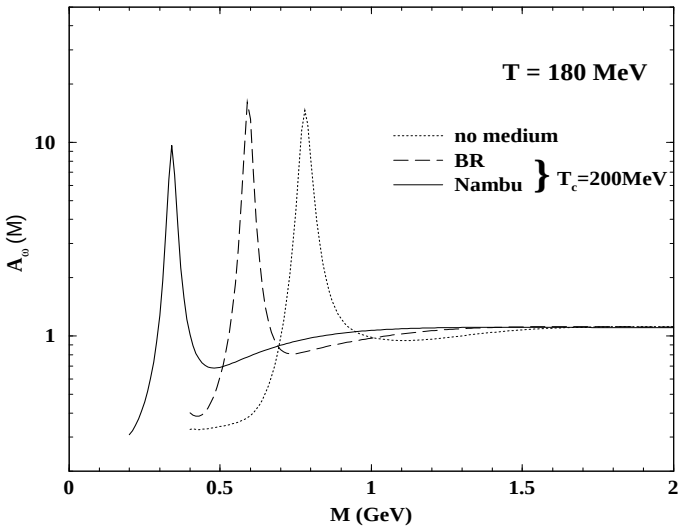

Figure 12: Same as Fig. 10 for the isoscalar channel.

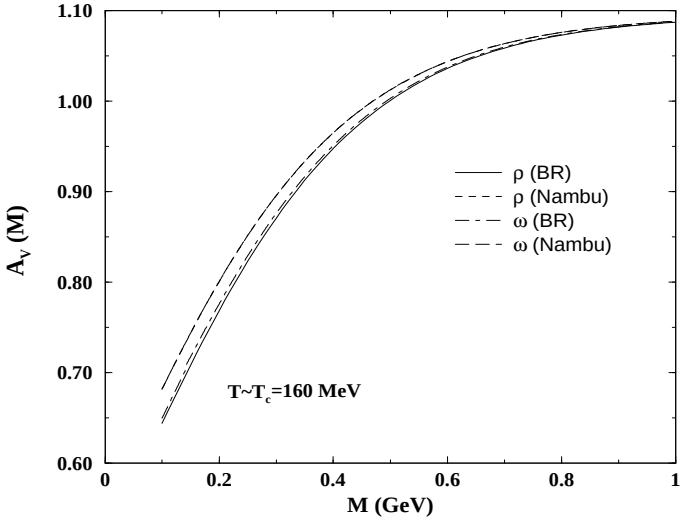

Figure 13: Spectral functions for isovector (ρ) and isoscalar (ω) channels at T_c .

7.2 Static photon spectra

In this section we consider the photon spectra from a hot hadronic matter and QGP. The medium effects enter through the masses and decay widths of the particles participating in the photon producing reactions. It is well known [15] that the reactions $\pi\,\rho \;\rightarrow\; \pi\,\gamma$, $\pi\,\pi \;\rightarrow\; \rho\,\gamma$, $\pi\,\pi \;\rightarrow\; \eta\,\gamma$, $\pi\,\eta \;\rightarrow\; \pi\,\gamma$, and the decays $\rho \;\rightarrow\; \pi\,\pi\,\gamma$ and $\omega \;\rightarrow\; \pi\,\gamma$ are the most important channels for photon production from hadronic matter in the energy regime of our interest. We have also included those reactions which produce photon via intermediary axial vector a_1 as discussed earlier. Non-zero width of vector and axial vector mesons in the intermediate state has been taken into account. While evaluating the photons from QGP we have considered both one loop and two loop contributions to the photon self energy as shown in Figs. (2) and (3).

The total photon emission rate from QGP and hadronic matter at $T = 160$ MeV is plotted in Fig. (14) as a function of the energy of the emitted photon for different values of strong charge g_s in the QGP phase and for various mass variation scenarios in the hadronic sector. The photon production rate from QGP has been evaluated in the HTL approximation, which is valid if the hard and soft scales are well separated, i.e. for $g_s << 1$ (which corresponds to $\alpha_s << 0.08$), whereas the QCD lattice calculations [123] suggest that $\alpha_s \sim 0.2 - 0.3$ at the temperature achievable in URHICs. This means that the extrapolation of results obtained under HTL approximation to higher values of g_s (or α_s) corresponding to lattice simulation may be dubious. We have evaluated the photon spectra for two values of the strong coupling constants $g_s = 0.8$ (solid square) and 2 (solid dots) to demonstrate the sensitivity of the photon spectra to the value of the strong charge and to show the uncertainties involved in the problem. In the hadronic sector the photon yield is seen to be enhanced compared to the case when the effects of the thermal interaction

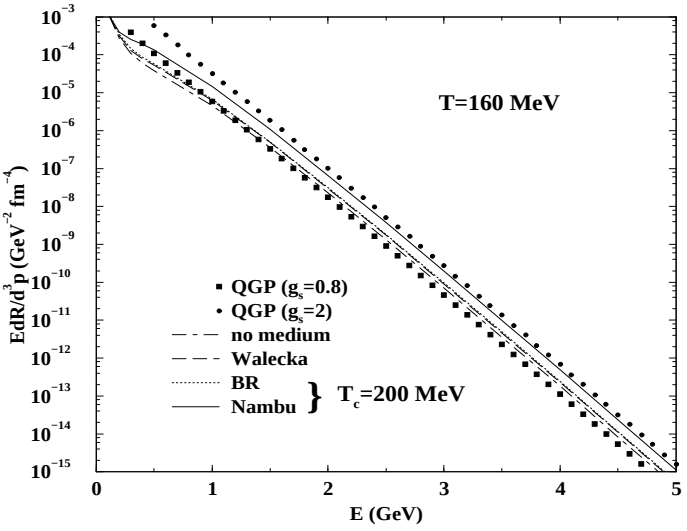

Figure 14: Thermal photon spectra at $T = 160$ MeV. Solid dots (square) indicates photon emission rate from QGP with both one loop and two loop contributions as evaluated by Kapusta et al and Aurenche et al respectively for $g_s = 2(0.8)$. Dotdash line represents photon spectrum from hot hadronic gas without medium effects. The result with the in-medium effects within the scope of the Walecka model calculations is shown by long dashed line. Dotted (solid) line indicates photon spectrum with BR (Nambu) scaling mass variation scenario.

on the hadronic properties are neglected. This is true for almost the entire energy range of the emitted photon under consideration. As a result of the similar mass shift in the Walecka model and BR scaling the photon spectra in these two scenarios (long-dashed and dotted lines respectively) have a negligible difference, whereas the enhancement in the spectrum due to hadronic mass shift according to Nambu scaling is clearly visible (solid line).

In Fig.(15) we show the photon emission rate at $T = 180$ MeV. Photon spectra from hadronic matter with mass variation according to the Nambu scaling scenario overshine the photons from QGP even for a larger value of g_s (~ 2).

Now the basic question is: At a fixed T which one is brighter – the hot hadronic gas or QGP?. Well, within the scope of the present work, the answer depends on (i) the value of the strong coupling constant, (ii) the degree of hotness of the medium and (iii) how adversely the hadrons are affected in the medium.

In Fig. (16) the effect of the form factor on the reaction $\pi\pi \to \rho\gamma$ has been demonstrated. We have taken same monopole form factor for both the $\pi\pi\rho$ and $\pi\pi\gamma$ vertices [15] to suppress the contribution from very high momentum region where the quark structure of the hadrons could be relevant. The Ward-Takahashi identity has been used to obtain the dressed propagator. The in-medium mass of the ρ meson has been taken from Walecka model calculations. The form factor effects for the above reaction reduces the photon production rate by about 10-15%. In view of the experimental uncertainty of the photon spectra measured in URHIC (*e.g.*

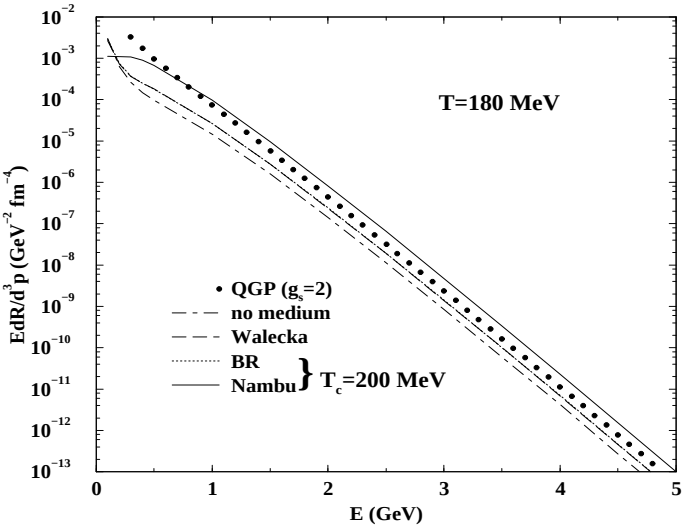

Figure 15: Same as Fig. (14) at $T = 180$ MeV and $g_s = 2$.

Ref. [124]) such effects are not relevant at present. Therefore, we have neglected it in the following discussions.

7.3 Static dilepton spectra

In Fig. (17) we display the invariant mass distribution of e^+e^- pair. The dilepton yield from $q\bar{q}$ annihilation is denoted by solid dots. Dotted line indicates the result obtained from the parameterization of the electromagnetic current-current correlation function in the 'ρ' and 'ω' channels, when the medium effects are ignored. A large shift towards the lower invariant mass region of the ρ peak is seen in the Nambu scaling (solid line) as compared to the BR scaling (dash line) consistent with the relative shift in the spectral functions in the two cases as discussed before. In the Walecka model calculations the relevant reactions are $\pi\pi \rightarrow e^+e^-$, $\rho \rightarrow e^+e^-$ and $\omega \rightarrow e^+e^-$ (dotdash line) [101, 102]. The two peaks corresponding to ρ and ω masses are visible in the spectra. The separation between the two peaks is due to different mass shift of the ρ and ω. Measurement of such separation in hadronic masses ($\Delta m = m^*_\omega - m^*_\rho$) would signal the in-medium effects. Validity of such results could be tested in URHIC by the CERES [125] collaboration in future. Similar shift at zero temperature but finite baryon density could be detected by HADES [126] and CEBAF [127]. Effects of the continuum on the dilepton spectra is clearly visible for $M \geq 1$ GeV (please note that the value of the continuum threshold in vacuum is 1.3 GeV). Due to the continuum contribution the dilepton rates from hadronic matter and QGP shine equally brightly in the mass range $M \geq 1$ GeV. The lepton pair spectra at $T = 180$ MeV is shown in Fig. (18). Since the effective mass of the rho in the Walecka and BR scaling scenario is almost same in this case (see Fig. (6)), the corresponding rates are very similar near the rho peak.

The dilepton invariant mass distribution at $T = T_c$ is shown in Fig. (19). All the

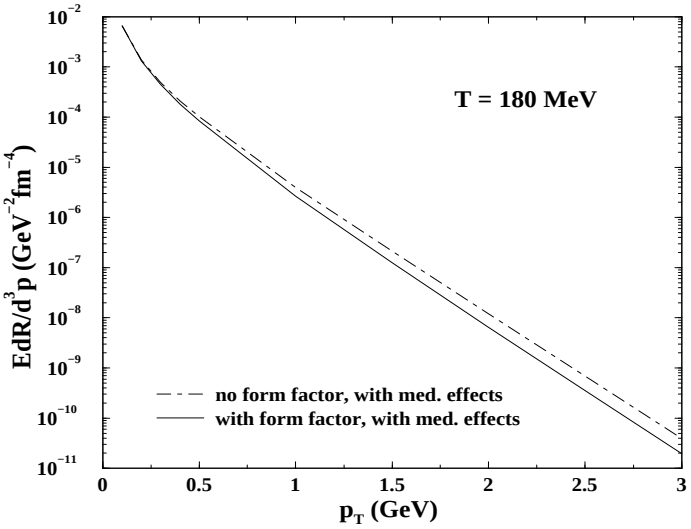

Figure 16: The effect of the monopole form factor on the photon emission rate from the reaction $\pi\pi \to \rho\gamma$.

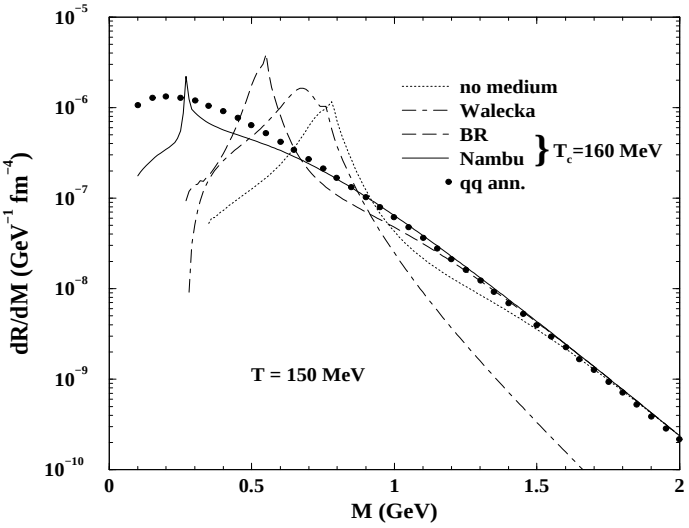

Figure 17: Thermal dilepton spectra at $T = 150$ MeV. Solid dots indicates dilepton emission rate from QGP. Dotted line represents dilepton yield from hot hadronic gas without medium effects. The result with the in-medium effects within the scope of the Walecka model calculations is shown dot-dashed line. Long dashed (solid) line indicates dilepton spectrum with BR (Nambu) scaling mass variation scenario.

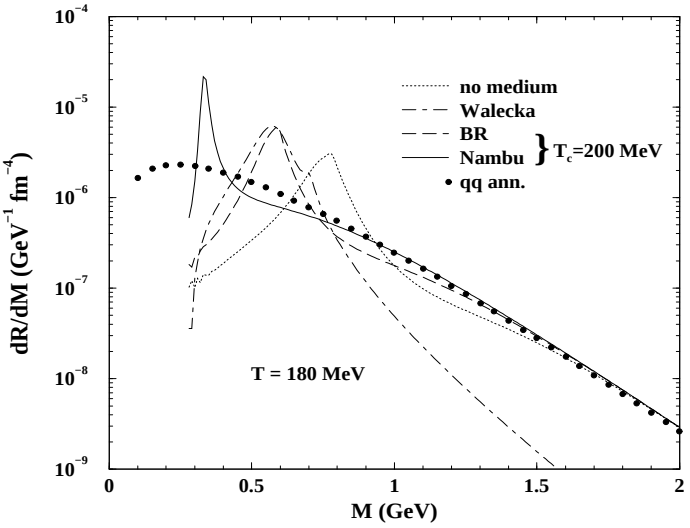

Figure 18: Same as Fig. (17) at $T = 180$ MeV.

peaks in the spectrum have disappeared as expected. The rates obtained from the electromagnetic current-current correlator is close to the rate from $q\bar{q}$ annihilation, indicating that the $q\bar{q}$ interaction in the vector channel has become very weak *i.e.* signaling the onset of deconfinement [128, 129].

7.4 Photon and dilepton spectra with space-time evolution

The basic aim of URHIC is to distinguish between the two possibilities:

A +A →(QGP)→(Mixed Phase)→Hadronic Phase or A + A →Hadronic Phase. The former (latter) case where the initial state is formed in QGP (hadronic) phase will be called the 'QGP scenario' ('no phase transition scenario'). In the following we will compare the photon and dilepton spectra originating from these two scenarios.

The observed photon and dilepton spectra originating from an expanding QGP or hadronic matter is obtained by convoluting the static (fixed temperature) rate with expansion dynamics. The basic ingredients required for a system undergoing rapid expansion from its initial formation stage to the final freeze-out stage with or without phase transition have been discussed in section 6. For the QGP sector we use a simple bag model equation of state (EOS) with two flavour degrees of freedom. The temperature in the QGP phase evolves according to Bjorken scaling law $T^3\,\tau = T_i^3\tau_i$. The cooling law in the hadronic sector is quite different from that of the QGP because of the presence of massive hadrons. These hadrons redress themselves in the medium thereby reducing their masses. This phenomenon must be taken into account in the evolution dynamics through the equation of state. We do this by introducing temperature dependence in the statistical degeneracy which takes care of the mass varying with temperature.

In Fig. (20) we depict the variation of effective degeneracy as a function of temperature with and without medium effects on the hadronic masses for various

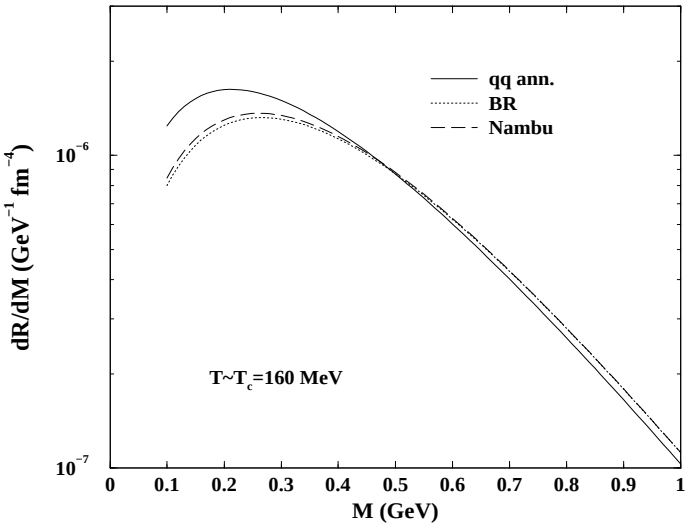

Figure 19: Same as Fig. (17) at $T = T_c$ MeV.

scenarios. We observe that for $T > 140$ MeV the effective degeneracy becomes larger due to the reduction in temperature dependent masses compared to the free hadronic masses. Physically this means that the number of hadrons in a thermal bath at a temperature T is more when in-medium mass reduction is taken into account. Eq. (6.20) implies that for a given pion multiplicity the initial temperature of the system will be lower (higher) when medium effects on hadronic masses are considered (ignored). This is clearly demonstrated in Fig. (21) where we show the variation of temperature with proper time for different initial conditions. The solid dots indicate the scenario where QGP is formed initially at $T_i = 185$ MeV and cools down according to Bjorken law up to a temperature T_c at proper time τ_Q, at which a phase transition takes place; it remains constant at T_c up to a time $\tau_H = 9.4$ fm/c after which the temperature decreases as $T = 0.247/\tau^{0.194}$ (when medium effects are taken from Walecka model) to a temperature T_f. If the system is considered to be formed in the hadronic phase then the initial temperature is obtained as $T_i = 220$ MeV (270 MeV) when in-medium effects on the hadronic masses from Walecka model is taken into account (ignored). The corresponding cooling laws are displayed in Fig. (21). The above parametrizations of the cooling law in the hadronic phase have been obtained by solving Eq. (6.11) self consistently. An initial state with the vanishing meson masses at $T_i = 195$ MeV ($\tau_i = 1$ fm/c) could be realised in the case of BR and Nambu scaling scenarios for the above value of pion multiplicity.

In Table 1 we quote the values of the initial temperatures obtained by assuming various mass variation scenarios. The value of initial thermalization time has been assumed as 1 fm/c both for SPS ($dN/dy = 600$) and RHIC ($dN/dy = 1735$) energies. τ_Q (τ_H) indicates the starting (end) point of the mixed phase. $\tau_H - \tau_Q$ is the life time of the mixed phase in a first order phase transition scenario. α and β dictate the variation of temperature with proper time for the hadronic matter according to

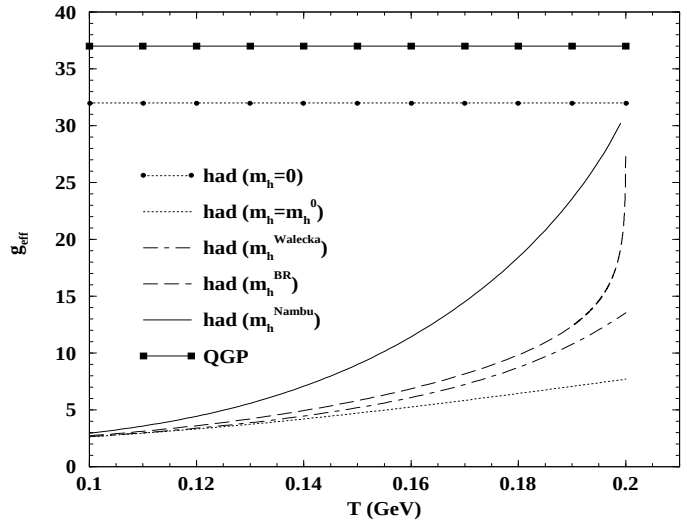

Figure 20: Variation of effective degeneracy as a function of temperature.

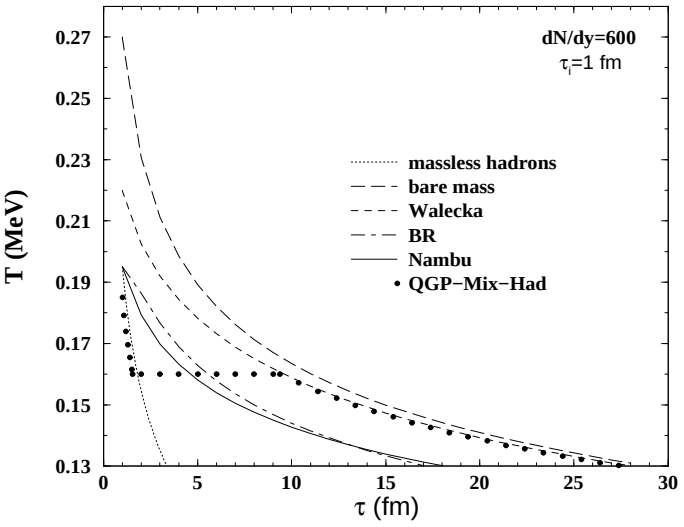

Figure 21: Variation of temperature as a function of proper time.

the cooling law $T = \alpha/\tau^{\beta}$. The values of β indicates a slower cooling in the hadronic phase as compared to that of QGP phase ($T \sim 1/\tau^{0.33}$).

	dN/dy=600 τ_i=1 fm				dN/dy=1735 τ_i=1 fm		
	hadronic gas initial state	QGP + Mix + Had T_i=185 MeV τ_Q=1.6 fm			QGP + Mix + Had T_i=265 MeV τ_Q=4.6 fm		
	T_i (MeV)	τ_H (fm)	α	β	τ_H (fm)	α	β
bare mass	270	10.8	0.267	0.215	31.9	0.337	0.215
Walecka	220	9.4	0.247	0.194	27.6	0.305	0.194
BR	195	8.2	0.236	0.184	23.9	0.288	0.185
Nambu	195	4.7	0.203	0.151	13.9	0.239	0.152

Table 1 : Values of initial temperatures and various time scales for SPS and RHIC energies.

Having obtained the finite temperature effects on hadronic properties and the cooling laws we now integrate the rates obtained in the previous sections over the space-time evolution of the collision. We must account for the fact that the thermal rates are evaluated in the rest frame of the emitting matter and hence the momenta of the emitted photons or dileptons are expressed in that frame. Accordingly, the integral over the expanding matter is of the form

$$\frac{dN}{d\Gamma} = \int_{formation}^{freeze-out} d^4x \frac{dR(E^*, T(x))}{d\Gamma} \tag{7.1}$$

where $d\Gamma$ stands for invariant phase space elements: d^3p/E for photons and d^4q for dileptons. E^* is the energy of the photon or lepton pair in the rest frame of the emitting matter and $T(x)$ is the local temperature. In a fixed frame like the laboratory or the centre of mass frame, where the 4-momentum of the photon or lepton pair is $q_\mu = (E, \vec{q})$ and the emitting matter element d^3x moves with a velocity $u_\mu = \gamma(1, \vec{v})$, the energy in the rest frame of the fluid element is given by $E^* = u_\mu q^\mu$.

In a first order phase transition scenario the photon and dilepton spectra from a $(1+1)$ dimensionally expanding system is obtained as

$$\begin{aligned}
\frac{dN}{d\Gamma} &= \pi R_A^2 \int \Bigg[\left(\frac{dR}{d\Gamma}\right)_{QGP} \Theta(s - s_Q^c) \\
&+ \Bigg[\left(\frac{dR}{d\Gamma}\right)_{QGP} \frac{s - s_H^c}{s_Q^c - s_H^c} \\
&+ \left(\frac{dR}{d\Gamma}\right)_H \frac{s_Q^c - s}{s_Q^c - s_H^c} \Bigg] \Theta(s_Q^c - s)\Theta(s - s_H^c) \\
&+ \left(\frac{dR}{d\Gamma}\right)_H \Theta(s_H^c - s) \Bigg] \tau \, d\tau \, d\eta
\end{aligned} \tag{7.2}$$

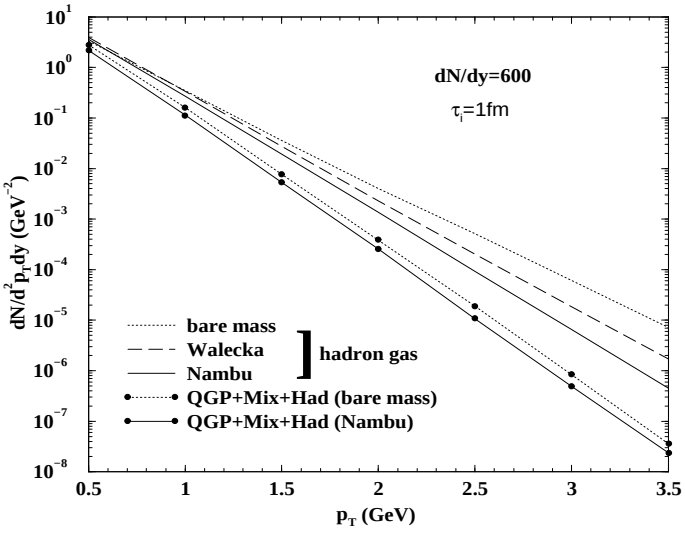

Figure 22: Total thermal photon yield corresponding to $dN/dy = 600$ and $\tau_i = 1$ fm/c. The solid (long-dash) line indicates photon spectra when hadronic matter formed in the initial state at $T_i = 195$ MeV ($T_i = 220$ MeV) and the medium effects are taken from Nambu scaling (Walecka model). The dotted line represents the photon spectra without medium effects with $T_i = 270$ MeV. The solid (dotted) line with solid dots represent the yield for the 'QGP scenario' when the hadronic mass variations are taken from Nambu scaling (free mass).

where R_A is the radius of the nuclei and Θ functions are introduced to get the contribution from individual phases.

As discussed earlier, $g_{\rm eff}$ is obtained as a function of T by solving Eq.(6.19). A smaller (larger) value of $g_{\rm eff}$ is obtained in the free (effective) mass scenario. As a result we get a larger (smaller) initial temperature by solving Eq.(6.20) in the free (dropping) mass scenario for a given multiplicity. Naively we expect that at a given temperature if a meson mass drops its Boltzmann factor will be enhanced and more of those mesons will be produced leading to more photons [52, 130]. However, a larger drop in the hadronic masses results in smaller initial temperature, implying that the space time integrated spectra crucially depends on these two competitive factors. Therefore, with (without) medium effects one integrates an enhanced (depleted) static rate over smaller (larger) temperature range for a fixed freeze-out temperature ($T_f = 130$ MeV in the present case). In the present calculation the enhancement in the photon emission due to the higher initial temperature in the free mass scenario (where static rate is smaller) overwhelms the enhancement of the rate due to negative shift in the vector meson masses (where the initial temperature is smaller). Accordingly, in the case of bare mass (Nambu scaling) scenario the photon yield is the highest (lowest). In case of the Walecka model, the photon yield lies between the above two limits. This is demonstrated in Fig. (22).

In the 'QGP scenario' the photon yield with in-medium mass is lower than the case where bare masses of hadrons are considered. However, the difference is

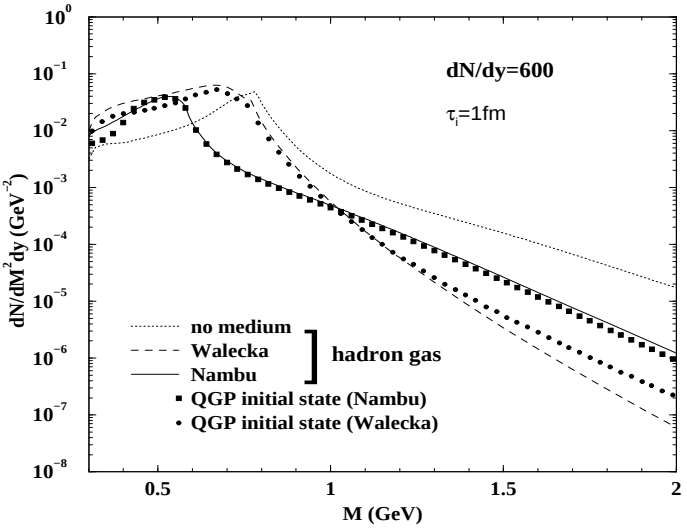

Figure 23: Total thermal dilepton yield corresponding to $dN/dy = 600$ and $\tau_i = 1$ fm/c. The solid (long-dash) line indicates dilepton spectra when hadronic matter formed in the initial state at $T_i = 195$ MeV ($T_i = 220$ MeV) and the medium effects are taken from Nambu scaling (Walecka model). The dotted line represents the spectra without medium effects with $T_i = 270$ MeV. The square (solid dots) line with solid dots represent the yield for the 'QGP scenario' when the hadronic mass variations are taken from Nambu scaling (Walecka model).

considerably less than the 'no phase transition scenario'. This is because, in this case the initial temperature is determined by the quark and gluon degrees of freedom and the only difference between the two is due to the different lifetimes of the mixed phase. In Fig. (22), the photon spectra from 'QGP scenario' is compared with that from 'no phase transition scenario'; the latter overshines the former.

The space time integrated dilepton spectra for the 'QGP scenario' and 'no phase transition scenario' with different mass variation are shown in Fig.(23). The shifts in the invariant mass distribution of the spectra due to the reduction in the hadronic masses according to different models are distinctly visible. Similar to the photon spectra, the dilepton spectra from 'no phase transition scenario' dominates over the 'QGP' scenario for invariant mass beyond ρ peak.

Finally we study the electromagnetic probes for RHIC energies. At RHIC a scenario of a pure hot hadronic system within the format of the model used here, appears to be unrealistic. The initial temperature considering bare hadronic masses turns out to be ~ 340 MeV whereas for the other extreme case of massless hadrons it is ~ 290 MeV. With temperature dependent masses the initial temperature will lie somewhere between these two values. For such high temperatures, clearly a hot dense hadronic system cannot be a reality, the hadrons would have melted away even for lower temperatures. Thus, for RHIC we have treated the case of a QGP initial state only. The temperature profile for RHIC is depicted in Fig. (24) where we observe that the length of the plateau, which indicates the life time of the mixed

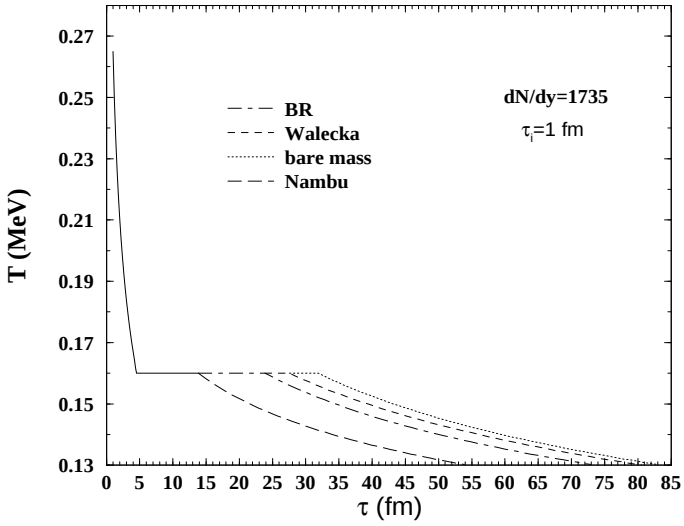

Figure 24: Variation of temperature as a function of proper time. The initial temperature has been determined by assuming 'QGP scenario'. The initial temperature $T_i = 265$ MeV for $\tau_i = 1$ fm/c and $dN/dy = 1735$

phase $\tau_{mix}^{life} = \tau_H - \tau_Q$, depends on the masses of the hadrons in the hadronic phase. The effective degeneracy plays an important role here. At the transition point there is a large decrease in the entropy density. This decrease has to be compensated by the expansion (increasing the volume) to keep the total entropy constant. Since we are considering (1+1) dimensional expansion this change in the entropy density will be compensated by increasing τ ($s\tau$ = const.). We have seen earlier (Fig. 20) that the effective degeneracy in the hadronic phase is the largest for the Nambu scaling and smallest for the bare mass scenario, resulting in smallest (largest) discontinuity in the entropy density for the former (latter) case. Consequently the time taken for the system to compensate the decrease of the entropy density in the Nambu scaling scenario is smaller as compared to bare mass case. Hence the life time of the mixed phase for the Nambu scaling case is smaller than all other cases.

The thermal photon yield for RHIC is displayed in Fig. (25). The solid line represents the total thermal photon yield originating from initial QGP state, mixed phase and the pure hadronic phase. The short dash line indicates photons from quark matter (QM) (= pure QGP phase + QGP part of the mixed phase) and the long dash line represents photons from hadronic matter (HM) (= hadronic part of the mixed phase + pure hadronic phase). In all these cases the effective masses of the hadrons have been taken from Nambu scaling. For $p_T > 2$ GeV photons from QM overshines those from HM since most of these high p_T photons originate from the high temperature QGP phase. The dotted and the dotdash lines indicate photon yields from QM and HM respectively with bare masses in the hadronic sector. The HM contribution for the bare mass is larger than the effective mass (Nambu) scenario because of the larger value of the life time of the mixed phase in the earlier case (see Table 1). It is important to note that for $p_T > 2$ GeV, the difference in

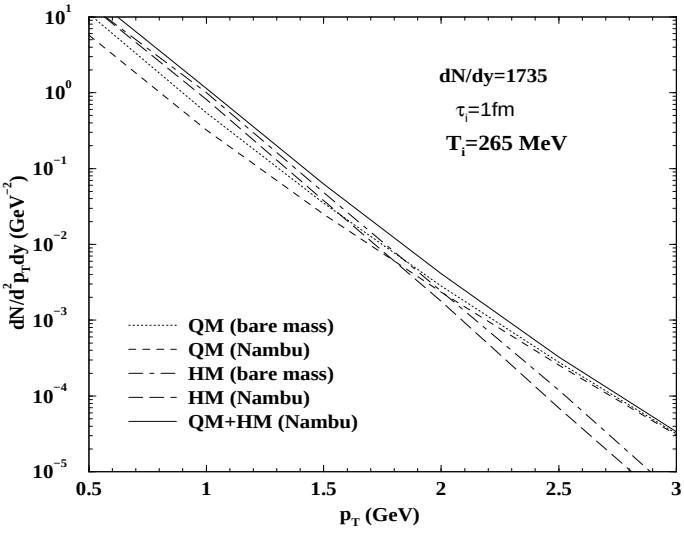

Figure 25: Thermal photon spectra at RHIC energies.

the QM and HM contribution in the effective mass scenario is more that the bare mass scenario.

Thermal dilepton yield at RHIC energies for QGP initial state and for different mass variation scenarios are shown in Fig. (26). The shape of the peak in the dilepton spectra in case of Walecka model is slightly different(broader) from the other cases because of the larger mass separation between ρ and ω mesons in this case (see Fig. (6)). The dilepton yield beyond the vector meson peak is larger in the bare mass scenario because of larger initial temperature (Table 1).

8 Summary and Outlook

In the present work we have reviewed the formulation of the production of photon and lepton pair from QGP and hot hadronic gas based on finite temperature field theory. The change in the spectral functions of the hadrons appearing in the internal loop of the photon self energy diagram have been considered in the Walecka model and QCD sum rule approach. The hadronic spectral functions (in vacuum) for the isovector and isoscalar channel have been constrained from experimental data on $e^+e^- \rightarrow hadrons$. Due to the lack of our understanding of the critical behaviour of scalar and tensor condensates we have parameterized the vector meson masses and continuum threshold as a function of temperature according to BR and Nambu scaling. Walecka model calculation shows different mass shift for ρ and ω mesons. The disentanglement of the ρ and ω peaks in the dilepton spectrum resulting from URHICs would be an excellent evidence of in-medium mass shift of vector mesons [125]. It has been observed that the in-medium effects on the dilepton and the photon spectra are prominently visible. The effects of the continuum on the dilepton spectra are seen to be substantial. In the present article the effects of hadronic mass

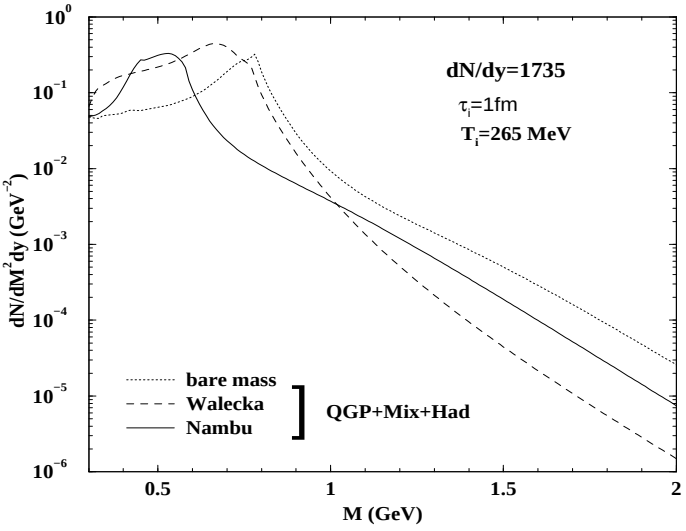

Figure 26: Thermal dilepton spectra at RHIC energies.

shift according to the non-linear sigma model and the hidden local symmetry model are not considered. Because in these models the mass reductions are not very large and consequently electromagnetic spectra will not be affected much from free space. The effect of the baryonic chemical potential is neglected in the present work, calculation addressing these issues is in progress [131].

The exact value of the critical temperature (T_c) for deconfinement phase transition is still uncertain. However, recent lattice simulation [4] for two flavour QCD indicates a value of T_c for chiral transition $\sim 130-160$ MeV. We have taken $T_c = 160$ MeV, although till now it is not known whether the values of T_c for the chiral and deconfinement transition are the same or not. The value of the initial thermalization time τ_i is unfortunately also an unknown quantity. We take $\tau_i = 1$ fm/c as a canonical value following Bjorken [105]. A similar value of τ_i has been considered in the literature, e.g. see Refs. [8, 130, 132].

The photon production from QGP has been considered using HTL resummation based on the assumption $g_s << 1$, which is impossible to meet in URHICs even at the highest energy to be available at CERN LHC in future. Therefore, the formidable task is to evaluate the photon spectra at the value of $g_s \sim 2$ likely to be attained by URHIC at RHIC/LHC.

In this respect the development of methods suitable for addressing non-perturbative effects near and above the QCD phase transition point is of paramount importance. Extension of the self-consistent resummation scheme developed in ϕ^4 theory [133] to non-abelian gauge theory [134, 135] would be a very important step towards the understanding of the phenomena near the QCD phase transition point.

Throughout this work we have assumed thermal equilibrium, which may not be realised practically [136, 137, 138, 139]. Unfortunately, although considerable progress has been made [140, 141, 142], the general techniques for solving non-equilibrium quantum field theoretical problems is still in the early stages of devel-

opment [143].

Acknowledgement: J. A. is grateful to Japan Society for Promotion of Science (JSPS) for financial support. T. H. was partly supported by Grant-in-Aid for Scientific Research No. 10874042 of the Japanese Ministry of Education, Science, and Culture. J. A. and T. H. were also supported by by Grant-in-Aid for Scientific Research No. 98360 of JSPS.

References

[1] J. C. Collins and M. J. Perry, Phys. Rev. Lett. **34** (1975) 1353.

[2] M. Kisslinger and P. Morley, Phys. Rev. **D10** (1976) 2765, 2771.

[3] E. V. Shuryak, Phys. Rep. **61** (1980) 71; Phys. Rep. **115** (1984) 151.

[4] A. Ukawa, Nucl. Phys. **A638** (1998) 339c.

[5] B. Müller, The Physics of Quark Gluon Plasma, (Springer, Heidelberg, 1985).

[6] R. C. Hwa (ed.), Quark Gluon Plasma 1 and 2, World Scientific, Singapore, 1990, 1995.

[7] C. Y. Wong, Introduction to High Energy Heavy Ion Collisions, (World Scientific, Singapore, 1994).

[8] J. Alam, S. Raha and B. Sinha, Phys. Rep. **273** (1996) 243.

[9] W. Cassing and E. L. Bratkovskaya, Phys. Rep., **308** (1999) 65.

[10] P. V. Ruuskanen, Nucl. Phys. **A 544** (1992) 169c.

[11] J. I. Kapusta, Nucl. Phys. **A 566** (1994) 45c.

[12] R. D. Pisarski, Phys. Lett. **B 110** (1982) 222; hep-ph/9503330.

[13] T. Hatsuda and T. Kunihiro, Phys. Rev. Lett. **55** (1985) 158; Phys. Lett. **B185** (1987) 304..

[14] T. Hatsuda and T. Kunihiro, Phys. Rep. **247** (1994) 221.

[15] J. I. Kapusta, P. Lichard, and D. Seibert, Phys. Rev. **D44** (1991) 2774.

[16] R. Baier, H. Nakkagawa, A. Niegawa and K. Redlich, Z. Phys. **C53** (1992) 433.

[17] P. Aurenche, F. Gelis, H. Zaraket and R. Kobes, Phys. Rev. **D 58** (1998) 085003.

[18] E. Braaten and R. Pisarski, Nucl. Phys. **B 337** (1990) 569; Nucl. Phys. **B339** (1990) 310.

[19] J. Frenkel and J. C. Taylor, Nucl. Phys. **B334** (1990) 199.

[20] U. Meissner, Phys. Rep. **161** (1988) 213.

[21] T. Hatsuda, Nucl. Phys. **A544** (1992) 27c.

[22] G. E. Brown and M. Rho, Phys. Rev. Lett. **66** (1991) 2720.

[23] M. Harada and A. Shibata, Phys. Rev. **D 55** (1997) 6716.

[24] A. Bhattacharyya, J. Alam, S. Raha and B. Sinha, Int. J. Mod. Phys. **A12** (1997) 5639.

[25] C. Song, Phys. Rev. **D 53** (1996) 3962.

[26] R. D. Pisarski, Phys. Rev. **D 52** (1995) 3773; Nucl. Phys. **A 590** (1995) 553c.

[27] E. Shuryak and V. Thorsson, Nucl. Phys. **A 536** (1992) 739.

[28] V. L. Eletsky, B. L. Ioffe and J. I. Kapusta, Nucl. Phys. **A 642** (1998) 155c.

[29] B. D. Serot and J. D. Walecka, Advances in Nuclear Physics Vol. 16 Plenum Press, New York 1986.

[30] S. A. Chin, Ann. Phys. **108** (1977) 301.

[31] C. Song, P. W. Xia and C. M. Ko, Phys. Rev. **C52** (1995) 408.

[32] E. Shuryak, Rev. Mod. Phys. **65** (1993) 1.

[33] M. A. Shifman, Prog. Th. Phys. (Suppl.) **131** (1998)1; hep-ph/9802214.

[34] G. E. Brown and M. Rho, Phys. Rep. **269** (1996) 333.

[35] E. L. Feinberg, Nuovo Cim. **34A** (1976) 39.

[36] P. V. Ruuskanen in Particle Production in Highly Excited Matter, eds. H. H. Gutbrod and J. Rafelski, (Plenum Press, New York, 1993)

[37] M. Le Bellac, Thermal Field Theory, Cambridge University Press, 1996.

[38] H. A. Weldon, Phys. Rev. **D42** (1990) 2384.

[39] L. McLerran and T. Toimela, Phys. Rev. **D31** (1985) 545.

[40] A. Das, Finite Temperature Field Theory, (World Scientific, Singapore, 1997).

[41] J. F. Nieves, Phys. Rev. **D 42** (1990) 4123.

[42] L. Dolan and R. Jackiw, Phys. Rev. **D9** (1974) 3320.

[43] L. S. Brown, Quantum Field Theory, Cambridge University Press, 1995.

[44] H. A. Weldon, Phys. Rev. Lett. **66** (1991) 293.

[45] H. A. Weldon, Ann. Phys. **228** (1993) 43.

[46] H. A. Weldon, Phys. Rev. **D 28** (1983) 2007.

[47] C. Gale and J. I. Kapusta, Nucl. Phys. **B357**, (1991) 65.

[48] V. B. Berestetskii, E. M. Lifshitz and L. P. Pitaevskii, Quantum Electrodynamics, Pregamon Press, 1982.

[49] R. Kobes and G. Semenoff, Nucl Phys. **B260** (1985) 714; **B272**, (1986) 329.

[50] F. Gelis, Nucl. Phys. **B508**, (1997) 483.

[51] C. Gale and J. I. Kapusta, Phys. Rev. **C35**, (1987) 2107.

[52] S. Sarkar, J. Alam, P. Roy, A. K. Dutt-Mazumder, B. Dutta-Roy, B. Sinha, Nucl. Phys. **A634**, (1998) 206.

[53] D. J. Gross, R. D. Pisarski and L. G. Yaffe, Rev. Mod. Phys. **53** (1981) 43.

[54] V. P. Nair, hep-th/9809086.

[55] J. P. Blaizot and E. Iancu, hep-ph/9903389.

[56] P. Aurenche, F. Gelis, H. Zaraket and R. Kobes, hep-ph/9903307.

[57] J. C. Taylor and S. M. Wong, Nucl. Phys. **B 355** (1990) 115.

[58] E. Braaten and R. D. Pisarski, Phys. Rev. **D 45** (1992) R1827.

[59] F. Flechsig and A. K. Rebhan, Nucl. Phys. **B464** (1996) 279.

[60] J. P. Blaizot and E. Iancu, Phys. Rev. Lett. **70** (1993) 3376.

[61] P. F. Kelly, Q. Liu, C. Lucchesi and C. Manuel, Phys. Rev. Lett. **72** (1994) 3461.

[62] V. V. Klimov, Sov. J. Nucl. Phys. **33** (1981) 934.

[63] H. A. Weldon, Phys. Rev. **D 26** (1981) 2789; Phys. Rev. **D 40** (1989) 2410.

[64] R. Baier, S. Peigne and D. Schiff, Z. Phys. **C62** (1994) 337.

[65] P. Aurenche, F. Gelis, R. Kobes and E. Petitgirard, Phys. Rev. **D54** (1996) 5274.

[66] A. Niegawa, Mod. Phys. Lett. **A 10** (1995) 379.

[67] A. Niegawa, Phys. Rev. Lett. **71** (1993) 3055.

[68] M. Gell-Mann, D. Sharp and W. D. Wagner, Phys. Rev. Lett. **8** (1962) 261.

[69] J. J. Sakurai, Currents and Mesons, The University of Chicago Press, Chicago, 1969.

[70] P. Roy, S. Sarkar, J. Alam and B. Sinha, Nucl. Phys. **A 653** (1999) 277.

[71] L. Xiong, E. V. Shuryak and G. E. Brown, Phys. Rev. **D46** (1992) 3798.

[72] C. Song, Phys. Rev.**C47** (1993) 2861.

[73] M. A. Halasz, J. V. Steel, G. Q. Li and G. E. Brown, Phys. Rev. **C 58** (1998) 365.

[74] J. K. Kim, P. Ko, K. Y. Lee and S. Rudaz, Phys. Rev. **D53** (1996) 4787.

[75] P. Ko and S. Rudaz, Phys. Rev. **D50** (1994) 6877.

[76] J. Alam and T. Hatsuda, to be published.

[77] S. Weinberg, Phys. Rev. Lett. **18** (1967) 507.

[78] J. I. Kapusta, Finite Temperature Field Theory, Cambridge University Press, 1993.

[79] N. P. Landsman and Ch. G. van Weert, Phys. Rep. **145** (1987) 141.

[80] A. A. Abrikosov, L. P. Gorkov and I. E. Dzyaloshinski, Sov. Phys. JETP **9** (1959) 636.

[81] E. S. Fradkin, Sov. Phys. JETP **9** (1959) 912.

[82] P. V. Landshoff, hep-ph/9808362.

[83] M. H. Thoma, hep-ph/9503400.

[84] P. Aurenche and T. Becharrawy, Nucl. Phys. **B379** (1992) 259.

[85] H. C. Jean, J. Piekarewicz and A. G. Williams, Phys. Rev. **C49**, (1994) 1981.

[86] J. C. Caillon and J. Labarsouque, Phys. Lett. **B311** (1993) 19.

[87] H. Shiomi and T. Hatsuda, Phys. Lett. **B334** (1994) 281.

[88] T. Hatsuda, H. Shiomi and H. Kuwabara, Prog. Th. Phys. **95** (1996) 1009.

[89] V. L. Eletsky and B. L. Ioffe, Phys. Rev. Lett. **78** (1997) 1010.

[90] A. I. Bochkarev and M. E. Shaposhnikov, Nucl, Phys. **B268** (1986) 220.

[91] T. Hatsuda and S. H. Lee, Phys. Rev. **C46** (1992) R34.

[92] T. Hatsuda, Y. Koike and S. H. Lee, Nucl. Phys. **B394** (1993) 221.

[93] L. J. Reinders, H. Rubinstein and S. Yazaki, Phys. Rep. **127** (1985) 1.

[94] B. L. Ioffe, Acta Phys. Polon. **B16** (1985) 543.

[95] M. Shifman (Ed.), Vacuum Structure and QCD Sum Rules, North Holland, Amsterdam, 1992.

[96] S. Narison, QCD Spectral Sum Rules, World Scientific, Singapore, 1989.

[97] M. Shifman, A. Vainshtein and V. Zakharov, Nucl. Phys. **B147** (1979) 385.

[98] N. V. Krasnikov, A. A. Pivovarov and N. N. Tavkhelidze, Z. Phys. **C19** (1983) 301.

[99] J. I. Kapusta and E. Shuryak, Phys. Rev. **D49** (1994) 4694.

[100] S. H. Lee, Phys. Rev. **C 57** (1998) 927; hep-ph/9904007.

[101] J. Alam, S. Sarkar, P. Roy, B. Dutta-Roy and B. Sinha, Phys. Rev. **C 59** (1999) 905.

[102] P. Roy, S. Sarkar, J. Alam, B. Dutta-Roy and B. Sinha, Phys. Rev. **C 59** (1999) 2778.

[103] M. Dey, V. L. Eletsky and B. L. Ioffe, Phys. Lett. **B252** (1990) 620.

[104] C. B. Chiu, E. C. G. Sudarshan and K. H. Wang, Phys. Rev. **D12**, (1975) 902.

[105] J. D. Bjorken, Phys. Rev. **D27**, (1983) 140.

[106] U. Heinz, P. Koch and B. Friman, Proc. Large Hadron Collider Workshop, Aachen (1990), CERN-90-10, Vol. II, p.1079.

[107] D. ter Haar (ed.), Collected papers of L. D. Landau, Gordon and Breach, London, 1965.

[108] P. Huovinen, P. V. Ruuskanen and J. Sollfrank, Nucl. Phys. **A650** (1999) 227.

[109] D. Yu. Peressounko and Yu. E. Pokrovsky, hep-ph/9906325.

[110] M. Asakawa and T. Hatsuda, Phys. Rev. **D55** (1998) 4488.

[111] See for example, Nucl. Phys. **A610** (1996).

[112] G. Q. Li, C. M. Ko and G. E. Brown, Nucl. Phys. **A606** (1996) 568.

[113] M. Asakawa, C. M. Ko, P. Levai and X. J. Qiu Phys. Rev. **C46** (1992) R1159.

[114] M. Herrmann, B. L. Friman and W. Nörenberg, Nucl. Phys. **A560** (1993) 411.

[115] G. Chanfray and P. Shuck, Nucl. Phys. **A555** (1993) 329.

[116] F. Klingl, N. Kaiser and W. Weise, Nucl. Phys. **A624** (1997) 527.

[117] B. Friman and H. J. Pirner, Nucl. Phys. **A617** (1997) 496.

[118] R. Rapp, M. Urban, M. Bubballa and J. Wambach, Phys. Lett. **B417** (1998) 1.

[119] W. Peters, M. Post, H. Lenske, S. Leupold and U. Mosel, Nucl. Phys. **A632** (1998) 109.

[120] G. E. Brown, G. Q. Li, R. Rapp, M. Rho and J. Wambach, Acta Phys. Polon. **B29** (1998) 2309.

[121] R. Rapp, G. Canfray and J. Wambach, Nucl. Phys. **A 617** (1997) 472.

[122] V. L. Eletsky and J. I. Kapusta, Phys. Rev. **C 59** (1999) 2757.

[123] F. Karsch, Z. Phys. **C38** (1988) 147.

[124] R. Albrecht et al, Phys. Rev. Lett. **76** (1996) 3506.

[125] I. Ravinovich, Nucl. Phys. **A638** (1998) 159c.

[126] http://piggy.physik.uni-giessen.de/hades/

[127] J. D. Walecka, Theoretical Nuclear and Subnuclear Physics, Oxford University Press, NY, 1995.

[128] E. V. Shuryak, hep-ph/9906443.

[129] R. Rapp, hep-ph/9907342.

[130] C. Song and G. Fai, Phys. Rev. **C58** (1998) 1689.

[131] S. Sarkar et al, under investigation.

[132] J. Sollfrank et al, Phys. Rev. **C55** (1997) 392.

[133] S. Chiku and T. Hatsuda, Phys. Rev. **D 57** (1998) R6; Phys. Rev. **D 58** (1998) 076001.

[134] J. O. Anderson, E Braaten and M. Strickland, hep-ph/9905337.

[135] J. P. Blaizot, E. Iancu and A. Rebhan, hep-ph/9906340.

[136] K. Geiger, Phys. Rep. **258** (1995) 237.

[137] X. N. Wang, , Phys. Rep. **280** (1997) 287.

[138] P. Roy et al, Nucl. Phys. **A 624** (1997) 687.

[139] H. Sorge, H. Stöcker and W. Greiner, Nucl. Phys. **A 498** (1989) 567c.

[140] A. Niegawa, Prog. Theor. Phys. **102** (1999) 1.

[141] M. Thoma, hep-ph/9808359.

[142] M. Burgess, hep-ph/9808116.

[143] K. Kajantie, Nucl. Phys. **A 610** (1996) 26c.